Quaternary Science Reviews 145 (2016) 204–225

Contents lists available at ScienceDirect

Quaternary Science Reviews

journal homepage: www.elsevier.com/locate/quascirev

Eastern Mediterranean sea levels through the last interglacial from a coastal-marine sequence in northern Israel

D. Sivan [a, *], G. Sisma-Ventura [a], N. Greenbaum [b, c], O.M. Bialik [d], F.H. Williams [e], M.E. Tamisiea [f], E.J. Rohling [g, e], A. Frumkin [h], S. Avnaim-Katav [a], G. Shtienberg [a], M. Stein [i]

[a] Department of Maritime Civilizations, L. H. Charney School of Marine Sciences and the Leon Recanati Institute for Maritime Studies (RIMS), University of Haifa, Mt. Carmel, Haifa, 3498838, Israel
[b] Department of Geography & Environmental Studies, University of Haifa, Mt. Carmel, Haifa, 3498838, Israel
[c] Department of Natural Resources & Environmental Management, University of Haifa, Mt. Carmel, Haifa, 3498838, Israel
[d] Dr. Moses Strauss Department of Marine Geosciences, Leon H. Charney School of Marine Sciences, University of Haifa, Mt. Carmel, Haifa, 3498838, Israel
[e] Ocean and Earth Science, University of Southampton, National Oceanography Centre, Southampton, SO14 3ZH, UK
[f] National Oceanography Centre, Liverpool, L3 5DA, UK
[g] Research School of Earth Sciences, The Australian National University, Canberra, 2601, Australia
[h] Institute of Earth Sciences, The Hebrew University, Jerusalem, 91905, Israel
[i] Geological Survey of Israel, 30 Malkhe Israel St., Jerusalem, 95501, Israel

ARTICLE INFO

Article history:
Received 8 January 2016
Received in revised form
16 May 2016
Accepted 2 June 2016

Keywords:
MIS5e sea levels
East Mediterranean
Galilee coast
Israel
Strombus bubonius
GIA modelling

ABSTRACT

A last interglacial (Marine Isotope Stage, MIS5e) marine-coastal sequence has been identified along the Galilee coast of Israel, with the type section located at Rosh Hanikra (RH). The microtidal regime and tectonic stability, along with the detailed stratigraphy of the RH shore, make the study region ideally suited for determining relative sea level (RSL) through the MIS5e interval in the eastern Mediterranean. The sequence contains fossilized microtidal subunits at a few meters above the current sea level. Unfortunately, all fossils were found to be altered, so that U-Th datings cannot be considered to represent initial deposition. We contend that U-Th dating of *Strombus bubonius* shells (recrystallized to calcite) suffices to indicate a lower limit of ~110 ± 8 ka for the time sea level dropped below the RH sedimentary sequence. The RH-section comprises three main subunits of a previously determined member (the *Yasaf Member)*: (a) a gravelly unit containing the diagnostic gastropod *Strombus bubonius* Lamarck (*Persististrombus latus*), which was deposited in the intertidal to super-tidal stormy zone; (b) *Vermetidae* reef domes indicating a shallow-water depositional environment; and (c) coarse to medium-sized, bioclastic sandstone, probably deposited in the shallow sub-tidal zone. The sequence overlies three abrasion platforms that are cut by tidal channels at elevations of +0.8 m, +2.6 m and +3.4 m, and which are filled with MIS5e sediments. We present a detailed study of the sequence, with emphasis on stratigraphic, sedimentological, and palaeontological characteristics that indicate sea-level changes. Although without precise absolute dating, the stratigraphic sequence of RH through MIS5e allows us to identify a time-series of RSL positions, using the elevations of three stratigraphic subunits. Reconstructed RSL values range from +1.0 m to +7 m (with uncertainly < 1 m), and most fall within a narrow range of +1.0 to +3.3 m. Toward the end of MIS5e, RSL exceeded about +7 m. Glacial isostatic adjustment (GIA) modelling using multiple ice histories suggests that GIA corrections range between about −1.8 m and +5.4 m. This implies that global mean sea level resided between −0.8 m and +8.7 m during most of MIS5e. The absolute GIA correction would not be constant through the interglacial, and reduces to a range of −1.2 m to+ 2.4 m towards the end of the interglacial.

1. Introduction

Reconstructed sea-level elevations and their age constraints show remarkable differences for MIS5e around the world, as does

* Corresponding author.
E-mail address: dsivan@research.haifa.ac.il (D. Sivan).

http://dx.doi.org/10.1016/j.quascirev.2016.06.001
0277-3791/

Table 1
Selected data of MIS5e sea levels (SLs) presenting differences between various databases.

	SL indicators and its elevation	Dating method	Age	Age uncertainty	Inferred SLs' through MIS5e	Vertical uncertainty	Curve structure	References	Remarks
Deep sea cores									
N. Atlantic and Equatorial Pacific	Benthic foraminiferal $\delta^{18}O$	Records beyond 40 kyr are dated by correlation to SPECMAP	135-115ka	The average is on the order of 0.5–0.8 ka	Above present day (0 m)	±13m		Waelbroeck et al. (2002)	
Red Sea	Benthic foraminiferal $\delta^{18}O$	For MIS52: synchronization with the high-resolution Antarctic records	~129–110 ka	centennial-scale for 25–70 kyr, and less for the Last Interglacial	Above present day (0 m)	±12m	One peak around 122 kyr.	Siddall et al. (2003)	Uplifted rates in Bab el Mandab of 0.02 m ka^{-1}
Red sea	Planktonic foraminiferal $\delta^{18}O$	Combining coral data with a new, continuous, SL reconstruction from recent calibration method for stable oxygen isotope record	~124-119ka	±1 ka and even smaller	Above +10 m.	±6 m to ±6.3	Fluctuating SL rising to the highest peak around 123ka, a short drop and another peak at 121.5ka	Rohling et al. (2008)	
Red Sea	Planktonic foraminiferal $\delta^{18}O$	Chronology independent of ice cores. Tie points with Soreq Cave record.	133-120ka	(±0.5 and ± 1 ka).	>0 m 126 to 130 ka (probability maximum curve, 95% confidence limits)	Fully propagated uncertainties expressed as vertical uncertainties maximum values of+/−3.4 m.	The probability maximum curve contains one peak at 127.8 ka; the raw data contains multiple oscillations through MIS 5e.	Grant et al., 2012, Grant et al. 2014	
Coral reefs									
Northeast Yucatan peninsula, Mexico	Complete coral reef-crest sequence at +3 m and +5.8 m.	^{230}Th mainly of the coral A. palmata colonies	~132–125ka ~121–118ka	Ages with values of 149 ± 8% $\delta^{234}U$were considered accurate to ±2 kyr	Prolonged SL at +2.5 m and rapid rise up to +6 m or even +9m	+3 m between ~126ka and 122ka and +6 m (between ~120 and 117kar	Two steps of long highstands: between ~126ka and 122ka and ~120 to 117ka	Blanchon et al., 2009	Stable area
West Australia	Fossil coral reefs	^{232}Th > 0:5 ppb	127-116ka	>3 ka	Between +2.2 and + 3.4 m up to 119–120 kyr and a jump up to +9.5m	Min. coral paleo-depth is 0.4 m in in-situ corals.	Two peaks; at 127ka, a jump to +3.4, highstand to about 120ka and a jump to +9.5 m at 120ka.	O'Leary et al., 2013; Hearty et al., 2007	Stable areas. GIA corrected palaeo SL
W. Australia, and the Bahamas	Coastal structures	U-series on corals and AAR of marine shells and whole rock	130 to 119ka	±2ka	Rise to standstill at +2.5 m ~(132 –~125ka), a fall and rise to standstill at +3.0 m–124 to~121ka and a jump to +6m–121 to 119ka)	±1 m.	Two highstand and a jump at the end	Hearty et al., 2007 (and refs therein)	Stable areas
Great Bahama bank	Coral reefs: a rise to +2 m, a drop and tidal notches at +6m	U-Th dating	132-118ka.		A rise to +2 m –132ka, stable at +2 m, a fall in ~125 ka, and restraining of reef growth to ~+2 m, and a notch at +6 m–118ka.		Two highstand and a jump at the end	Chen et al., 1991; Neumann and Hearty, 1996;	Tectonically stable.
Hawaii and Bermuda	Coral reefs	U-Th (TIMS)	From ~134 to ~113 ka, with most ages	Between ±0.6ka to ±3ka	High stand at +8.5 to + 12.5 m			Muhs et al., 2002; Hearty et al., 2007	

(*continued on next page*)

Table 1 (*continued*)

	SL indicators and its elevation	Dating method	Age	Age uncertainty	Inferred SLs' through MIS5e	Vertical uncertainty	Curve structure	References	Remarks
			between ~125 and ~115 ka		(Hawaii), +2 to +3 m (Bermuda)				Slightly uplifting in Hawaii and stable in Bermuda
Pacific Coast - Isla Guadalupe, Baja California	Coral reef terraces	U-Th (TIMS)	~125,000 kyr		+1 to +6-m but shallow-marine or beach sediments are found up to +13 m			Muhs et al., 1994	Presumed to be tectonically stable
Barbados	Three coral reef terraces during MIS 5e,	ESR and TIMS (U/Th)	ESR: 132-118ka, U-Th: 128-120ka	±0.6 kyr to ±1ka (U/Th) 5-9ka(ESR)	Uplifted +20-+40 m		Three stands	Schellmann and Radtke, 2004	Assuming a constant uplift rate of 0.276 m/ka
Haiti	+5 m and +2 m,	U/Th	~130 and 118 ka		+5 m at 130.5 ka, +2.7 m for the second ~117.9ka but more probably ~ 123−122 ka.		Two stands	Dumas et al., 2006	Assumed constant uplift − different rates for different terraces
Huon Peninsula (New Guinea),			~134 ka and 118 ka				Two high stands	Stein et al., 1993	Tectonically active
Seychelles Islands, Indian Ocean	+1.7 and + 6 m *Goniastrea* and *Porites*	U-Th (TIMS)	131ka to 122ka,		Coral buildup to 131ka followed by sea level drop between 131 and 122ka.		Single high stand	Israelson and Wohlfarth, 1999	Relatively stable
Coastal structures in the Mediterranean									
Almeria, S. Spain	Marine terraces containing *Strombus bubonius*	U series of Mollusks, mainly of *Strombus bubonius* in different elevations of 0.5 m, 4 m and 11m	From 132ka and on (also MIS5c ages)	Up to ±14ka.				Hillaire-Marcel et al., 1986	Tectonically active.
Spanish coasts, mainly the Canary Islands, Alicante province and Balearic Islands	Marine terraces containing "Senegalese fauna" including *Strombus bubonius,*	12 new U-series measurements of shells (SB, Patella and Thais) and the coral *Cladocora caespitosa* by TIMS	100.6 to 138.4ka (with previous data: 135 to 117 ka)	1.3 to 3.4ka			Three highstands during MIS 5e.	Zazo et al., 2003	Tectonically active. Uplifted subsidence rated were calculated.
The southeastern coasts of peninsular Spain, the Balearic and Canary Islands	Marine terraces containing "Senegalese fauna" including *Strombus bubonius* at elevations of +2 m to +3 m.	Mostly U-series (α and TIMS) measurements of mollusk shells, AAR and OSL.					Three highstands the second of which is considered the most stable (~130 −120 ka).	Zazo et al., 2013 (and refs therein)	Tectonically active
Spain: La Marina-El Pinet site (Alicante)	Progradation of a barrier spit that grew during the MIS 5e	The study relies on previous U-series measurements on mollusk shells and corals.			No absolute SL elevation − only relative vertical fluctuations.			Dabrio et al., 2011	
Mallorca Island								Hillaire-Marcel et al., 1986; Hearty, 1987; Zazo et al., 2002	
Gibraltar	+5.0 m based on notch, caves,shelters, ledges, and a bioerosive	U/Th datings on *Acanthocardia tuberculata* shells	~114.5−110 ka	Shell − open system. ±6.5−7.3ka	Rapidly reached height of +5 at the beginning of MIS5e			Rodríguez-Vidal et al., 2007	A mean uplift value of 0.05 + 0.01 mm/year from 200 kyr (Rodríguez-Vidal et al., 2007).

	procession and regression to +1.5 m, with small tidal benches								
Cyprus	*Cladocora caespitosa* corals at ≤+3 m	U series	130 and 116 ka	±2ka			Fluctuations - two SL high peaks.	Pool et al., 1990	The area is tectonically active
Baal-en-Naame, Lebanon	Marine conglomerate with SB and *Vermetidae* overlain by *SB* unit at +10 m. In 3 places it is overlain by breccia that contains Levallois technique artifacts also covered by another *Vermetidae* layer up to +10.5 m	U series			+7 m and +10 m, a retreat and another relatively long phase of +8.5 m highstand followed by shorter highstand at 10.5m		Fluctuations - two SL high peaks.	Sanlaville, 1971	The area is tectonically active
N.Galilee, Israel		Stratigraphy and paleontological correlation.	MIS5e					Sivan et al., 1999	Tectonically stable.
Site location	**SL indicators and its elevation**	**Dating method**	**Age**	**Age uncertainty**	**Inferred SL**	**vertical uncertainty**	**Curve structure**	**References**	**Remarks**

the character of its variability (Table 1). MIS5e fossil coral reefs indicate an extended period between about 134 ka and 116 ka when sea level stood higher than present day (e.g. Muhs et al., 2002; Dutton and Lambeck, 2012; Marino et al., 2015; Hibbert et al., 2016). Although sea-level elevations derived from these indicators generally range between +2 and + 8 m in stable areas (e.g. Chen et al., 1991; Neumann and Hearty, 1996; Dumas et al., 2006; Blanchon et al., 2009; Dutton and Lambeck, 2012), various different patterns have been documented for MIS5e relative sea-level variability (Table 1). These include a single peak at ~5 m above present sea level (Chen et al., 1991; Muhs et al., 2002), two highstands of +2.5 m and +6 m up to +9 m (Stein et al., 1993; Neumann and Hearty, 1996; Stirling et al., 1998; Hearty and Neumann, 2001; Schellmann and Radtke, 2004; Dumas et al., 2006; Hearty et al., 2007; Blanchon et al., 2009; O'Leary et al., 2013), multiple high-stands of up to about +20 m based on benthic oxygen isotope data from deep-sea cores (Waelbroeck et al., 2002), and a double or triple peak up to about +10 m in the Red Sea (Rohling et al., 2008; Grant et al., 2012).

New MIS5e studies remain critical for understanding past sea level, and they have the potential radically change past interpretations, even in previously studied locations. In Western Australia, sea-level indicators were interpreted in terms of a prolonged flat highstand through MIS5e (Dutton and Lambeck, 2012), but subsequent research inferred that relative sea level in this area comprised an initial highstand, controlled by glacial isostatic adjustment (GIA) processes, followed by a sharp upward jump (O'Leary et al., 2013). Further, Long et al., 2015 contrast the multiple records of mid to low latitude RSL change during MIS5e with high-latitude records for northwest Europe that display no major RSL oscillations for this period. Although Long et al. (2015) model the North Sea region as being potentially insensitive to rapid ice mass loss in Greenland, the study raises valid questions regarding the source of RSL oscillations during MIS5e.

Sea-level reconstruction, notably of the last ~0.5 Myr, relies on: (a) shallow water corals (e.g. *Acropora palmata*; Fairbanks, 1989); (b) benthic foraminiferal $\delta^{18}O$ values in deep-sea cores (e.g. Waelbroeck et al., 2002); (c) strongly amplified surface-water $\delta^{18}O$ changes in evaporative marginal seas resulting from water residence-time changes due to sea-level driven modifications to cross-sectional strait-passages in the Red Sea (Siddall et al., 2003; Rohling et al., 2009; Grant et al., 2012) and the Mediterranean (Rohling et al., 2014); and (d) elevation of coastal structures and macro-fauna (Table 1). All methods contain uncertainties and inaccuracies in both elevations and dating. Fossil-coral-based sea-level indicators offer the best (radiometric) age constraints to RSL records. Such well-dated, non-altered coral reefs are commonly reported to record sea level with vertical uncertainties of up to 5 m (Fairbanks, 1989), although assemblage studies claim greater precision. Instead, coastal sedimentary structures can offer more precisely constrained indicators of past sea level when carefully related to the depositional environments and corrected for local tectonics (Hearty et al., 2007, Table 1), but are generally less well dated.

In the Mediterranean Sea, there are no corals that can be used as sea-level indicators. Here the key fossil indicator for MIS5e is the gastropod *Strombus bubonius*. It is now known as *Persististrombus latus* (Taviani, 2014), but we retain the old synonym for ease of comparison with referenced literature (e.g., Zazo et al., 2003, 2013 and references therein; Bardaji et al., 2009, Sivan et al., 1999). *Strombus bubonius* is part of the so-called Senegalese fauna, which indicates a relatively warm coastal and littoral environment (Bardaji et al., 2009; Murray-Wallace and Woodroffe, 2014, p. 283). The fossil coral *Cladocora caespitosa*, which often is associated with *Strombus*-bearing terraces, has been dated mainly to MIS5e using Amino-acid and U series methods (Hearty et al., 1986a; Zazo et al.,

2003 and references therein). Unfortunately, *Cladocora caespitosa* is not suitable for use as a sea-level indicator because of its large depth-habitat distribution. Based on this association, *Strombus*-bearing terraces are commonly attributed to MIS5e (Sivan et al., 1999; Bardaji et al., 2009; Zazo et al., 2003, 2013), although they also occur in terraces assigned to MIS7 in the western Mediterranean (Zazo et al., 2013 and references therein). Such MIS5e terraces have been identified along the Spanish coast (Hoang and Hearty, 1989; Zazo et al., 2003, 2013; Bardaji et al., 2009; Dabrio et al., 2011), in Mallorca (Hillaire-Marcel et al., 1986; Hearty, 1987; Zazo et al., 2002), in the Gibraltar region (Rodríguez-Vidal et al., 2007) (Table 1), and in Calabria and Puglia, Italy (Hearty et al., 1986b; Dumas et al., 2005). Elevations of these marine terraces vary between +1.5 and + 5 m. In Mallorca, MIS5e RSL was also reconstructed from coastal cave speleothems, between +1.5 and + 3 m (Tuccimei et al., 2006; Dorale et al., 2010).

In the eastern Mediterranean, indications for rapid RSL changes within MIS5e have been documented in the Gulf of Corinth, Greece. These include microbial bioherms with inter-grown marine coralline algae at elevations of 10–20 m over a marine terrace (Andrews et al., 2007). These terraces have potentially been affected by tectonic movements (Pavlopoulos et al., 2012), so that the data cannot be used for reconstructing a high-resolution RSL curve. In Cyprus, U-Th ages of *Cladocora caespitosa* corals in marine terraces, at elevations ≤+3 m, range between 108 ± 6 and 138 ± 4 ka, in broad agreement with MIS5e (Pool et al., 1990).

Along the Galilee coast of northern Israel (Fig. 1), a marine bioclastic, calcareous sandstone – the "*Yasaf*" Member (Mb) – has been previously related to MIS5e (Sivan et al., 1999). Coastal outcrops have been recognized in many patches, with thicknesses ranging from a few cm to 2 m. *Yasaf* Mb. sediments extend up to ~150 m inland of the present coastline, and reach an elevation of about +5 m. Dating the *Yasaf* Mb. by U-Th of mollusc shells has failed, since all were found to have been altered into calcite. Hence, the *Yasaf* Mb. has been assigned to MIS5e based on local stratigraphy and correlation to *Strombus*-bearing units elsewhere in the Mediterranean (see above; Sivan et al. (1999), and references therein). A similar unit bearing Senegalese fauna (Zazo et al., 2003, 2013; Bardaji et al., 2009) has been documented along the Carmel coast of Israel (Galili et al., 2007), where it was dated using optically

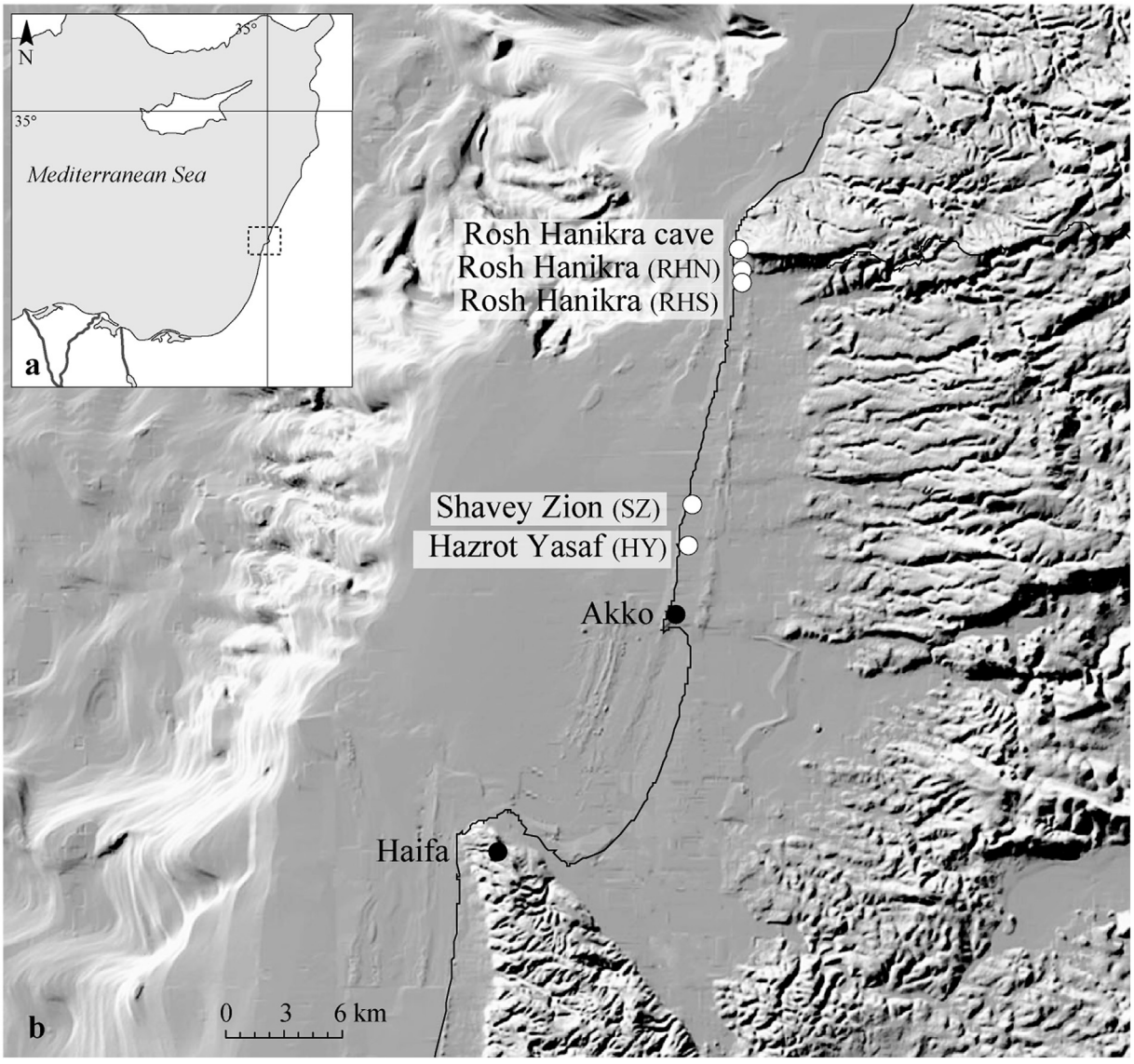

Fig. 1. Location map: a. The Israeli coast, East Mediterranean, b. The northern coast of Israel - study area and sites: Hazrot Yasaf (HY), Shavey Zion (SZ), Rosh Hanikra south (RHS), Rosh Hanikra north (RHN) and the cave locations.

stimulated luminescence (OSL) to 113 ± 5 ka (Mauz et al., 2012).

In Lebanon, conglomerate terraces composed of large rounded pebbles and containing *Strombus bubonius* are exposed along the coast, similar to the sections investigated here. In Na'ame, Beirut bay, Lebanon, a +7 to +10 m marine terrace is overlain by a marine *Strombus bubonius* unit, and there is a fossilized, calcareous bench with *Vermetidae*. In places, it is overlain by breccia that contains Levallois (Middle Palaeolithic stone knapping) artifacts that is again covered by a *Vermetidae* layer up to +10.5 m. The *Vermetidae* layers indicate MIS.5e relative sea levels of +7 m and +10 m (Sanlaville, 1971). The *Strombus* and *Vermetidae* units were radiometrically dated to between 93 and 90 ka (Bar-Yosef, 1998), while the Levallois artifacts were dated by Thermoluminescence (TL) and Electron Spin Resonance (ESR) to between 140 and 80-75 ka (Bar-Yosef, 2007). The Lebanese area has been affected by late Holocene vertical tectonic movements of at least 1–1.5 m, associated with episodic earthquakes (Sivan et al., 2010 and references therein), so that the Na'ame section cannot serve as an accurate sea-level marker.

In contrast, the Israeli coast is thought to be tectonically stable, based on geological research (Sneh, 2000) and comparison of Holocene archaeological sea-level indicators along the Carmel coast (Galili et al., 2007) and the Galilee coast with model predictions (Sivan et al., 2001, 2004, 2010). This tectonic stability makes the Galilee coast suitable for obtaining relative sea-level records of wider significance.

Here, we report results from a shore sequence in Rosh Hanikra, northern Israel, which includes a gravel unit with *Strombus bubonius* fossils that is overlain by a *Vermetidae* reef, and which is in turn covered by bioclastic sandstone. Our new sedimentological and palaeontological data provide a relative sea-level record with small vertical error bars through MIS5e on the Galilee coast. The in-situ and in growth position *Vermetidae* reef is a strong indicator of low-energy sea conditions. A major effort was made to date the *Strombus bubonius* fossils, but the U-Th results seem indicative only of alteration ages. Therefore, our sequence provides information on continuous relative sea-level fluctuations (with assumed uncertainty $\leq$ 1 m) through time, which are of wider significance due to the region's tectonic stability (Table 2), despite a lack of precise absolute age control. We combine our proposed chronostratigraphy and accurate elevations with modelled GIA predictions for the location, to compare our sea-level reconstruction with other global records.

2. Materials and methods

We surveyed sites on the Galilee coast, including sites in which *Strombus bubonius* fossils were previously found (Sivan, 1996; Sivan et al., 1999), with new indications in Rosh Hanikra. Detailed surveys and sampling (Fig. 1) were performed along west to east cross sections (Fig. 2), perpendicular to the coastline, at three sites: Hazrot Yasaf, Shavey Zion, and Rosh Hanikra north (RHN) and south (RHS). Another outcrop was documented within the Rosh Hanikra sea cave located in RHN, where the Rosh Hanikra ridge gives rise to vertical sea cliffs (Fig. 1). For accurate documentation, the survey uses RTK Proflex 500 GPS with horizontal and vertical precisions of one and five cm, respectively. The sea cave outcrop was surveyed using a Leica Disto laser distance meter and inclinometer and a hand-prismatic compass, with horizontal and vertical precisions of five cm. All data are related to the Israeli Land Survey Datum. Stratigraphic correlations between sites were established (Fig. 3) using the sedimentological characteristics and elevations of the subunits. The field exposures of each unit are presented in Fig. 4.

We document several subunits within the *Yasaf* Mb. bioclastic sandstone, which overlies the *Regba* Mb. calcareous sandstone that is locally named kurkar (Sivan, 1996; Sivan et al., 1999). A complete stratigraphic section with all subunits was found only in Rosh Hanikra north. Therefore, we propose the RHN site as the type section for the Last Interglacial in Israel. The *Yasaf* Mb. subunits comprise a *Strombus* subunit, a *Vermetidae* reef, an algal crust, and lower and upper bioclastic sandstone (Fig. 3). All were deposited in shallow marine environments (Table 2).

The subunits of the *Yasaf* Mb. were deposited on a palaeotopographic surface of *Regba* Mb. sandstone and are inclined seaward. Deposition occurred between present sea level and a few meters above present sea level, with indications of transgression and regression in each depositional phase (Fig. 3). The upper bioclastic sandstone in Rosh Hanikra was excavated during historical periods for building blocks (Fig. 4c 17: and 18), which provided a detailed 3-dimensional outcrop of the upper part of the sequence. These excavations also exposed the other subunits, such as the *Vermetidae* reef identified in the current study. The various subunits are exposed to a lesser extent at the other sites: Hazrot Yasaf and Shavey Zion (Fig. 4a and b). In the Rosh Hanikra sea cave within in the chalky E-W Rosh Hanikra ridge (Fig. 1), we identified both the *Strombus* subunit and the bioclastic sandstone subunit (Fig. 4c: 19–21).

Each subunit (Table 2) was sampled for petrographic analysis, carbonate content, and microfaunal identifications, in the case of the mound-shaped reef structures, to determine the various depositional conditions. Grain size analyses were carried out in the field and under the microscope. Pebble-sized and larger gravels were measured in the field, corroborated by measurements on size-calibrated photos. Short-axis lengths of fine grains were measured under the microscope, relative to a calibrated micrometer. From each interval, when possible, two subsamples of at least 90 grains were measured for each grain type (quartz, calcareous and pebbles); subsamples with less than 30 grains were not used (Fig. 5).

For petrographic analyses, eighteen thin sections were prepared and analyzed for the coastal sites, and four from the cave. The thin sections were cut perpendicular to the horizon for optimal coverage (Fig. 6). Thin sections were analyzed using an Olympus BX53-P petrographic microscope, and their structures were classified following Wright (1992). Diagenetic features were classified and interpreted following compilations by Moore (1989), Tucker and Wright (1990), Flügel (2010) and references therein. Samples were powdered, dried and inorganic carbon content was measured using a Primacs SLC analyzer.

For microfossil analyses, the partially indurated sediments were sampled and treated with warm H_2O_2 to improve disaggregation. After dry weighing, sediments were wet-sieved over a 63 μm mesh and dried at room temperature; the >63 μm fraction was used for foraminiferal and ostracod analyses. The taxonomy used in speciation of the benthic foraminifera is based mainly on Cimerman and Langer (1991), Hottinger et al. (1993), Sgarrella and Moncharmont-Zei (1993), Jones (1994), and Reiss et al. (1999). Total and relative benthic foraminiferal abundances were determined, and species diversity was expressed as raw diversity (species richness). The identification of ostracod taxa is based mainly on Athersuch et al. (1989), Maddocks et al. (2004) and Mischke et al. (2014). The preservation state of foraminifera and ostracods was evaluated based on several criteria (e.g., breakage, reworking, population structure, sorting, articulation of ostracods shells) indicating taphonomic processes within the depositional environment (e.g., Frenzel and Boomer, 2005).

One sample of the *Regba* Mb. sandstone underlying the *Yasaf* Mb. was OSL dated. Due to the low dose rate (0.405 ± 0.030 Gy/ka), chemical analyses for dose rate calculations were replicated. Considering that the equivalent dose of 87 ± 5 Gy is well below saturation of the OSL signal, we consider the age reliable.

For the main (*Yasaf* Mb.) sequence, the *Strombus* sub-samples

Table 2
Field description of the *Yasaf Mb*. subunits, elevations and inferred MIS5e sea levels relative to present day. Reconstructed global mean sea levels are calculated by applying the maximum range of modelled GIA corrections.

Unit	Thickness [m]	Minimum elevation (m)	Maximum elevation (m)	Sedimentology	Depositional settings	Infered palaeo-sea-level	Inferred global mean sea level)GMSL(
Upper bioclastic sandstone			6.45 RHS 3.9 HY 5.2 SZ	Pebbles at base, medium grained poorly sorted bio-clastic sandstone with abundant shell fragments and spicules (Echinodermata). Isopachous cement fill and dissolutions.	Shallow sub-tidal	Maximum SL at ~ +6.5–7.0 m.	Using RSL indicator of +7 m GMSL inferred using the wider set of GIA corrections is between +4.7 m and +12.4 m. Using the range of GIA corrections for the end of the interglacial GMSL is constrained within +5.8 m and 9.4 m.
Lower bioclastic sandstone		0.93 SZ 1.0 HY 1.1 RHS		Marine bio-clastic sandstone. Unconformable contact at base. Well-bedded dipping seaward. Rhodolithes, coarse bioclastic: gastropods, bivalves, and vermetids. Some grains exhibit micritic envelopes inter granular blade cement and granular cements.	Shallow sub-tidal variable energy	Rising SL	N/A
Unconformity				End of dissolution features and quartz grain occurrence, irregular contact.			
Algal crust	0.13 in the measured spot (see picture)	2.78 at RHN (on the Domes).	1.96 RHS 2.78 RHN	Undulatory to cumulate algal/microbial buildup with low degree of inheritance. bioclastic fragments: bivalve, red algae, formaminifera and small gastropods. Fine silt quartz grains.		The same SL (as of the domes) at ~+3m	GMSL between +1.2 m and +8.4 m.
Vermetidae domes (Only in RHN)	Average (of 5): 0.43	1.08	Base: 2.33 Top: 2.78	Mound shape structure constructed of The photographs seem to show indeed *Petaloconchus glomeratus* (Linnaeus, 1758), Fam. Vermetidae and encrusting calcareous algae. Poorly or well rounded, and poorly sorted bioclastic fragments: bivalve and red algae. Fine silt quartz grains. Granular cement fill and various dissolution features.	Shallow sub-tidal to intertidal high energy	Standstill, SL at ~+3 m	GMSL between +1.2 m and +8.4 m.
Strombus bearing sub unit	Varied	0.8 RHN 0.9 RHS 0.96 SZ	1.75 RHN 1.75 RHS 2. 4 HY	Patchy conglomerate, unconformably overlying the *Regba*. Poorly sorted, coarse gravel unit composed of subrounded-rounded cobbles and few bolders, fine silt quartz and bioclasts: mollusks, algae, bryozoan, foraminifera (miliolids), Rhodolithes 5–8 cm in size, *Vermatus Sp., Strombus bubonius* LMK (now termed *Lentigo latus)* and unidentified gastropods. Granular cement fill and various dissolution features.	Intertidal to super-tidal storm-generated	Sea level rose to ≥ ~+ 1.0 up to 2,5–3.0 m.	GMSL between −0.8 m and +8.4 m.
Unconformity				Irregular contact.		Sea level fall to ≤0.8 m.	GMSL between −1 m and +6.2 m.
Regba Mb.		Lower terrace (1) is at present: 0.8 −0.9 m. the second (2): is at 2.05	Upper terrace (3) is at:3.33	Aeolinite calcareous sandstone, cross-bedded: primarily troughs. The top consists of planar fine laminas slightly dipping seaward. Fine silt quartz, bioclasts, and calciclastics micrite and red algae, at times with micritic envelopes. Varius dissolution features and intergranular cements The upper surface is eroded.	Aeolian with indications of coastal environment at the top.	The MIS 5e sea level rose to ~+1.0 m, than to ~+2 m, and to ~ +3.3 m creating abrasion platforms.	GMSL between −0.8 m and +8.7 m.

and other fossil samples (Table 3) were crushed to powder and spiked with a mixed ^{229}Th-^{236}U spike. U and Th were separated by column chemistry following procedures in Vaks et al. (2007) and Torfstein et al. (2009). U and Th isotopes were analyzed by Nu plasma ICP-MS-MC at the Geological Survey of Israel. The ^{234}U/^{238}U (atomic) ratio obtained for NBL112a over the course of this study was $(5.299 \pm 0.004)\cdot 10^{-5}$ ($\pm 2\sigma$; n = 21).

During a glacial-interglacial climate cycle, sea level changes in response to the growth and melting of large land-based ice sheets (Emiliani, 1955). The loading and unloading of land surfaces and ocean basins mean that the sea level measured in any given location will not reflect the global average (Farrell and Clark, 1976; Milne and Mitrovica, 2008). GIA modelling allows us to investigate both the local relative sea level (RSL) and the global mean sea level (GMSL) change in response to a prescribed change in ice volume. We define the GIA correction as the difference between GMSL and RSL.

The GIA response at the study site (Rosh Hanikra; 33.093°N, 35.105°E) is modelled using a range of Earth models and eight global ice-loading histories that cover a range of glacial-interglacial ice volumes. We vary spatial dispersal patterns for the ice volume, as well as the duration of the interglacial between ice histories, to investigate the GIA response to a broad series of assumptions, as summarized in Table 4. Further detail on the GIA, ice and Earth

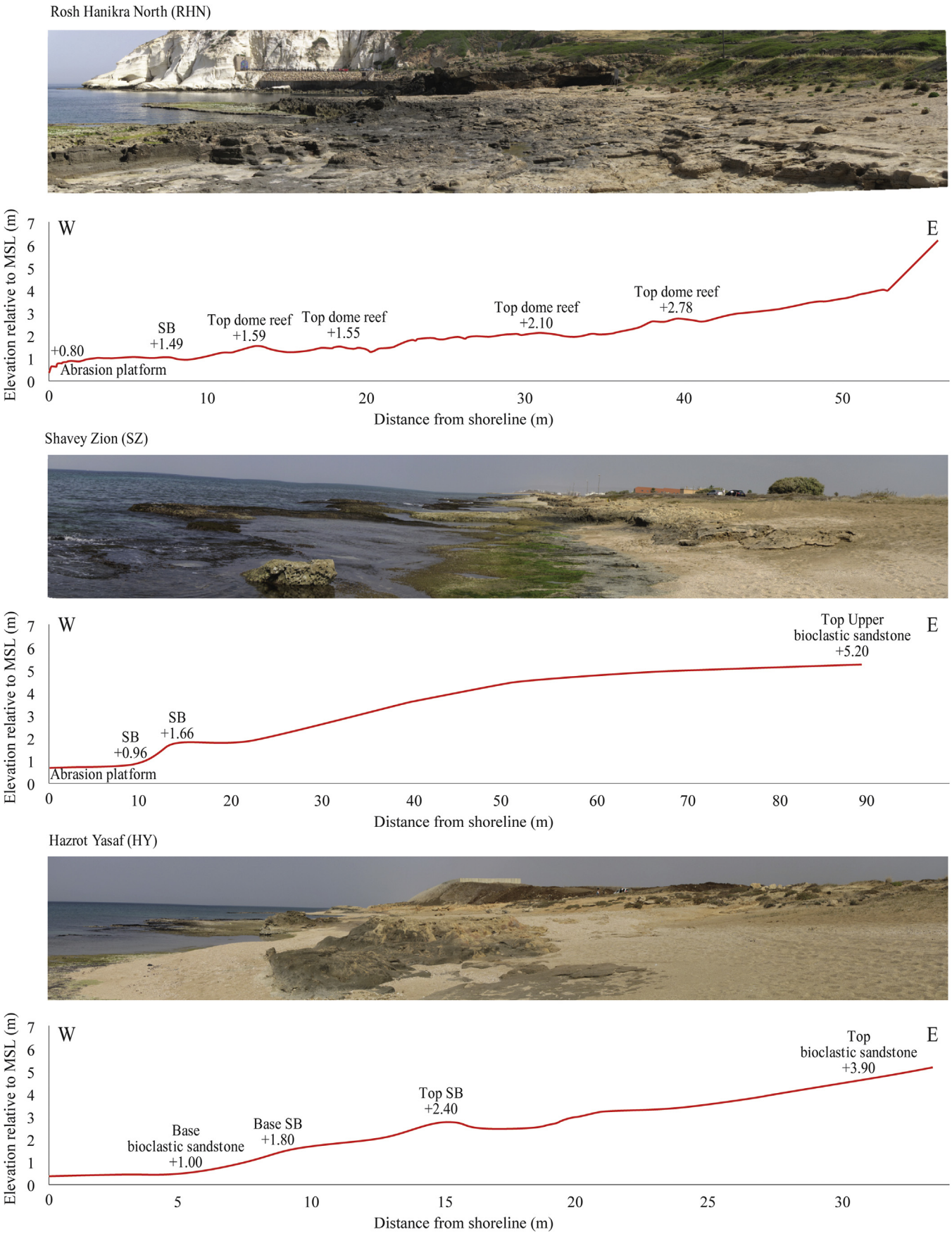

Fig. 2. Cross sections, from west to east, of three selected study sites on the Galilee coast, Israel, with elevations and panoramic views.

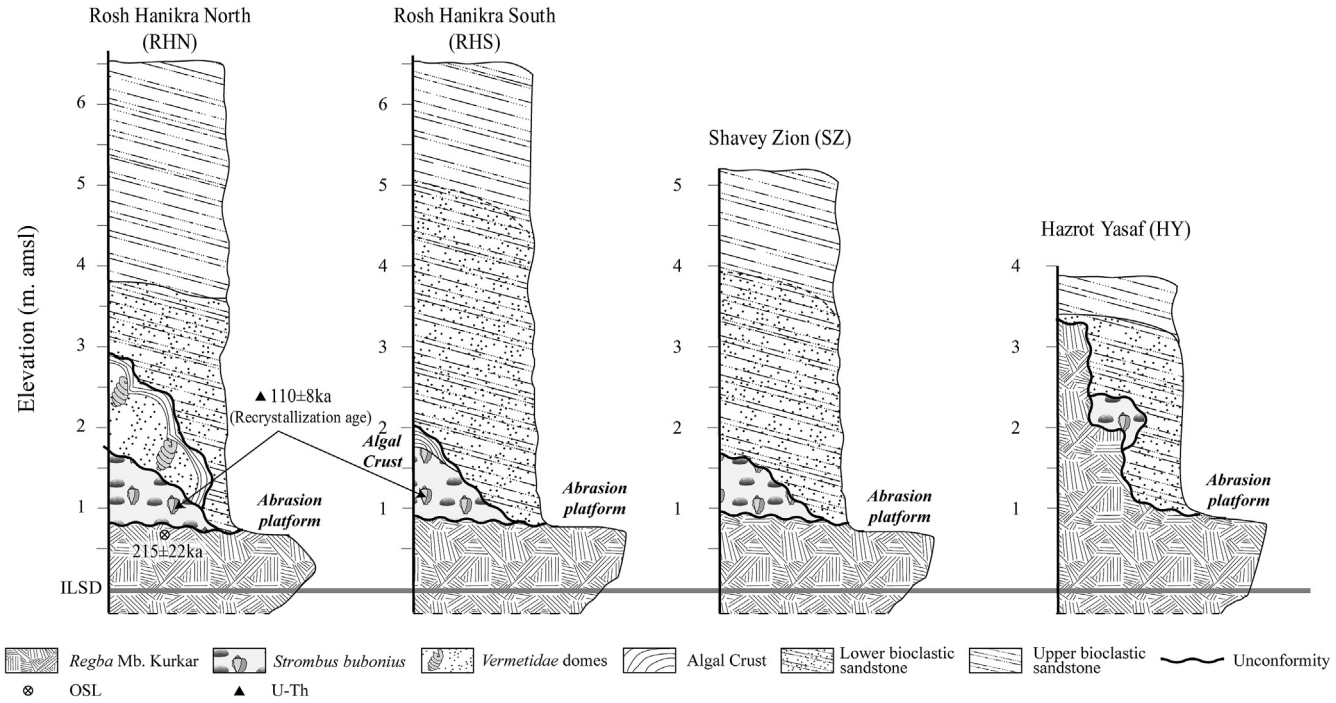

Fig. 3. Lithology and stratigraphical relations for the four study sites along the coast. The top of the lower *Regba Member* (Mb) is calcareous sandstone (locally named kurkar), dated for the first time in the current study to MIS7. Three abrasion platforms were cut into the *Regba* Mb by MIS5e sea (Fig. 4a; 1 and 4a; 2). On top of the *Regba* Mb. the *Strombus bubonius* bearing subunit is unconformably deposited. The *strombus* subunit is overlain, only in Rosh Hanikra North (RHN), by the *Vermetidae* dome shaped mounds (Fig. 4b: 9 and 4b:10) themselves covered by algal crust (Fig. 4b:13 and 4b:14). Where the domes are missing, e.g. in Rosh Hanikra South (RHS), the algal crust directly overlies the *strombus* subunit (Fig. 4b14 and 4b15). Two bioclastic sandstone beds unconformably overlie the domes, the lower is coarser and less sorted while the upper sandstone is finer and better sorted. In places, coarser and finer bioclastic sandstones alternate with each other in the contact zone.

models can be found in the supplementary material (Supplement Figures S1 and S2).

To create the ice histories, we first adapt a version of the ICE-5G ice history (Peltier, 2004) so that it covers two glacial cycles (Ice 1). Ice 1 approximates the MIS 6 to MIS 5e transition by reproducing the ICE-5G deglaciation from last glacial maximum to present day. Ice histories 2 and 3 represent a global model of ice volume variation based on the Red Sea RSL reconstruction (Grant et al., 2014). We use ICE-5G and the de Boer et al. (2014) three-dimensional ice history as a template for the spatial distribution of ice within Ice 2 and Ice 3 respectively. To investigate the impact of duration of the interglacial on the predicted GIA corrections, we insert either an artificial 4-kyr highstand (Ice 2a and 3a), or an 8-kyr highstand (Ice 2b and Ice 3b) at the peak interglacial point. The coral record provides a strong indication that MIS5e contained an extended period in which sea level was at a higher level than present day (Dutton and Lambeck, 2012; Medina-Elizalde, 2013; Hibbert et al., 2016), and these higher sea levels may require global ice volume to be smaller than today (Kopp et al., 2009). As mentioned before, quantifying the number of sea-level oscillations and their sources remains problematic (see also Dutton et al., 2015; Long et al., 2015). We therefore adapt our ice histories to model a single extended highstand, of varying duration, and of less than present day ice volume.

A key difference between Ice 2 and Ice 3 is that Ice 2 contains about 25 m of sea-level equivalent volume in the maximum Eurasian ice sheet, whereas Ice 3 contains approximately 40 m of sea-level equivalent volume in the Eurasian ice sheet at maximum volume. Evidence for a MIS 6 Eurasian ice sheet of greater volume and distribution than at the Last Glacial Maximum is provided by the QUEEN project (Svendsen et al., 2004). This model was constrained with observational evidence for sea level, and incorporated into a GIA ice history by Lambeck et al. (2006). The combination of a larger Eurasian ice sheet with a smaller Laurentide ice sheet at MIS 6 has since been found to be compatible with models of past climate (Colleoni et al., 2016).

Ice 4 is based on a model-generated 3-dimensional ice history (de Boer et al., 2014). Ice 5 is based on a deep-sea benthic $\delta^{18}O$ stack (Lisiecki and Raymo, 2005), with a scaling of maximum and minimum ICE-5G ice volume mapped to maximum and minimum $\delta^{18}O$ values between the last glacial maximum and present day. Finally, Ice 6 is based on a global mean sea-level curve that was derived from deep-sea benthic $\delta^{18}O$ from multiple ocean basins with adjustments based on selected fossil coral data (Waelbroeck et al., 2002).

3. Results

3.1. Field observations

In all Galilee coast sites (Figs. 1 and 2), the *Regba* Mb. calcareous sandstone forms the base of the sequence (Sivan et al., 1999). This sandstone forms a coastal ridge that is exposed to the west (seaward side) at sea level and becomes topographically higher to the east (landward). It is characterized by large-scale cross bedding, and is considered to be an aeolianite (Fig. 4a) (Sivan et al., 1999). This aeolianite is overlain in places by low-angle, tabular, planar laminae of the bioclastic sandstone (upper part of the *Yasaf* Mb.), which dip slightly seaward and are thought to reflect a shallow marine to coastal environment (Figs. 4a, 3 and 4 and Table 2).

The current abrasion platform consists of *Regba* Mb. sandstone, which is being abraded by modern tidal channels (Fig. 4a 1). Two higher abrasion platforms are apparent in the Hazrot Yasaf site (Fig. 3), at elevations of +2.6 (Figs. 4a and 2) and +3.4 m, respectively (Table 2). These contain palaeo-tidal channels filled with the upper bioclastic sandstone sediments of the *Yasaf* Mb (Fig. 4a: 2).

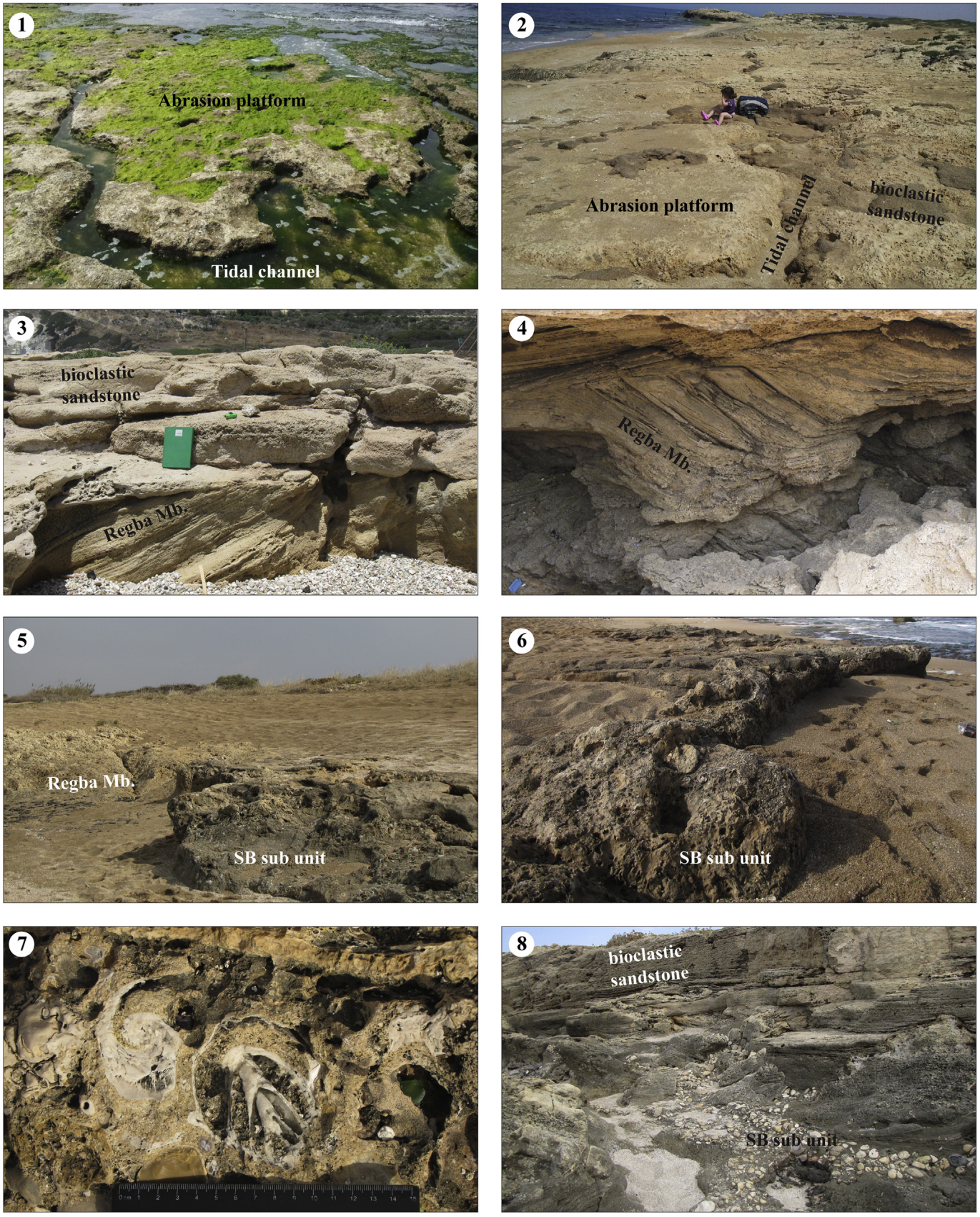

Fig. 4. Field exposures indicating the characteristics and the stratigraphical relations of the subunits; 4a: 1. Modern abrasion platform cutting the *Regba* Mb. sandstone, with tidal channels. 4a:2. Probable MIS5e abrasion platform at Hazrot Yasaf (HY), at an elevation of +2.0 m (Table 2) with tidal channels filled with the bioclastic sandstone deposits. 4a:3. *Regba* Mb. thin laminae tilting seaward (RHN). 4a:4. The lower exposures of the *Regba* Mb. tilting laminae indicate aeolianite, while the upper part can be interpreted as shallow marine sand bar. 4a:5. A patchy *Strombus bubonius* bearing in Shavey Zion (SZ) on a *Regba* Mb. relief. 4a:6. Closer view of the *Strombus* subunit in SZ, containing also large pebbles and macro-fauna. 4a:7. Typical *Strombus bubonius* fossils and pebbles. 4a:8. The *Strombus* subunit, which in places mainly consists of pebbles (RHS). 4b: 9. Dome shaped mounds, mainly of *Petaloconchus*, in RHN. 4b:10. Close-up of one of the mounds. Dome thickness can reach ~0.5 m (Table 2). 11. *Vermetidae* patches overlying the *Strombus* subunit in HY where they do not build dome shaped mounds. 4b:12. Close-up of *Petaloconchus*. 4b:13. The algal crust directly overlying the *Strombus* subunit in RHS. 4b:14. Close-up of the algal crust. 4b:15–16. The bioclastic sandstone unit that unconformably overlies the *Regba* Mb. in SZ. The bioclastic sandtone is thick and massive, but becomes more patchy inland. 4c:17–18 Overview from north to south of the bioclastic sandstone subunit in RHN. The sandstone has been quarried in historical periods, in most places up to the *Regba* Mb. but is preserved in the wall along the coast that the excavators left as a protection from the sea spray. This remnant wall enables to estimate the original volume of the bioclastic sandstone. 4c:19. The *Strombus* and sandstone subunit in the sea cave within the Cretaceous chalk cliff, Rosh Hanikra, north to RHN. 4c:20–21 The bioclastic sandstone base in the cave at elevations ranging from +1.5 m to +4.0 m, with thickness of about 1.1 m.

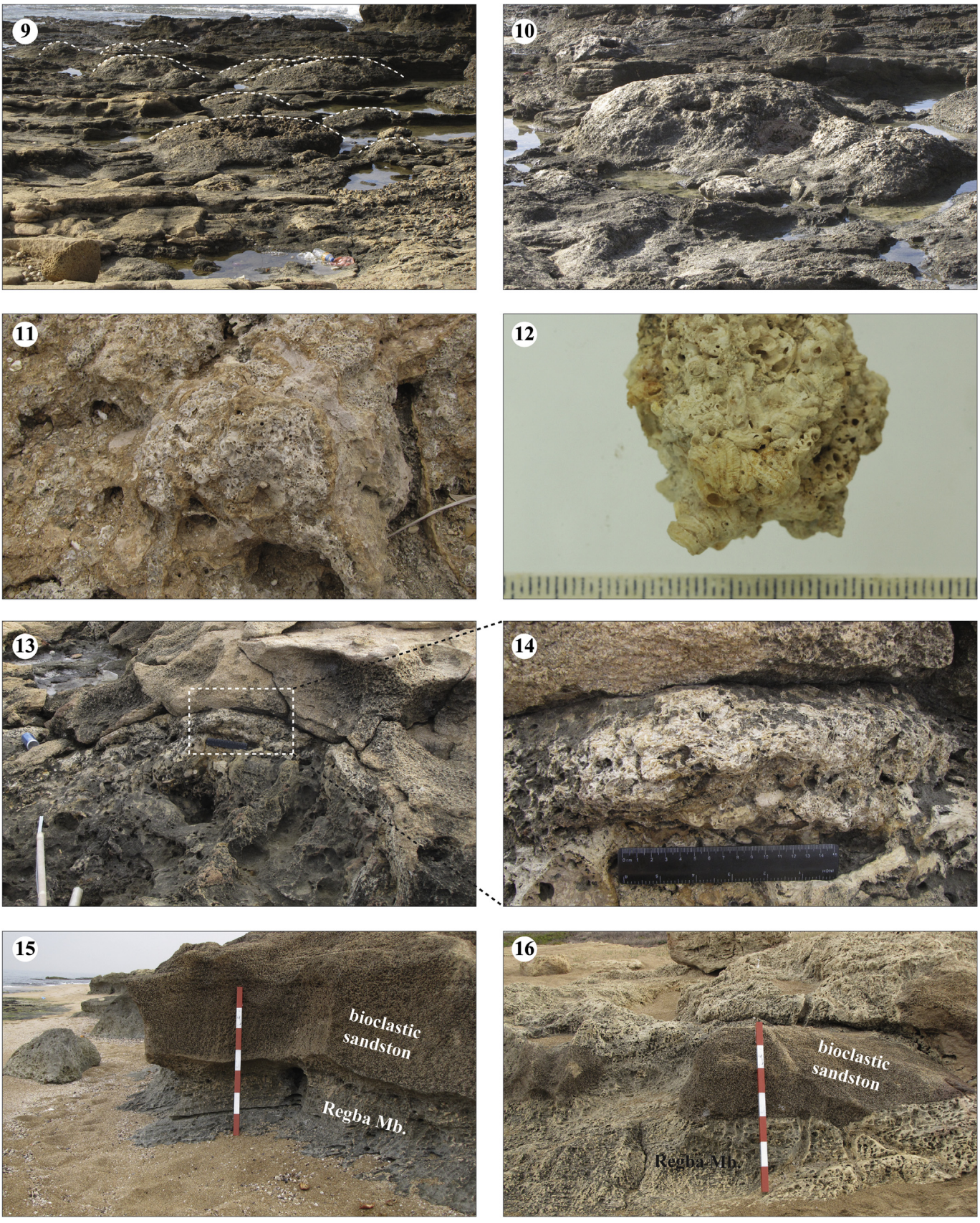

Fig. 4. (*continued*).

Fig. 4. (*continued*).

and indicate two steps of sea-level rise within MIS5e. The first rise abraded the platforms while later a terminal MIS5e rise caused infill with the upper bioclastic sandstone.

The oldest unit that unconformably overlays the *Regba* Mb. sandstone is the *Strombus* subunit (Table 2 and Fig. 3), a gravel unit containing sub-rounded limestone, chert, and sandstone pebbles in a matrix of fragmented macro- and micro-bioclasts. The *Strombus* subunit contains a warm Senegalese marine gastropod fauna (Zazo et al., 2003 and references therein) dominated by *Strombus bubonius* (Fig. 4a:5 to 4a:8). This subunit has been found at all study sites (Figs. 1 and 3) in the form of very hard conglomerate patches that directly overlay the *Regba* Mb. Sandstone, from the elevation of the present-day abrasion platform at RHS and SZ, up to maximum elevations of +2.4 m at HY, +1.75 m at RHN and RHS, and +1.66 m at SZ (Fig. 3 and Table 1). In the sea cave, the chalky bedrock is unconformably overlain by patches of this marine conglomerate, containing matrix-supported, rounded to subangular gravel-size clasts, mainly pebbles and cobbles, with some marine molluscs. There, it is found at elevations from modern sea level to about +1 m (Fig. 4c: 19–21).

Overlying the *Strombus* subunit is the *Vermetidae* subunit, with base elevations between +1.08 and + 2.33 m. This subunit consists of mound-shaped bioherms ("domes") (Fig. 4b9 and 4b10) constructed by colonies of *Vermetidae* (Fig. 3 and Table 2). The domes were found only at RH, and their thickness varies between 0.3 and 0.5 m. They consist primarily of *Petaloconchus* (Fig. 4b:11 and 4b:12). The mound shapes are coated by composite algal microbialite crusts with a thickness of about 0.13 m (Fig. 4b:13 and 4b:14 and Table 1). These crusts cover either the *Vermetidae* bioherms, or the *Strombus* subunits where the *Vermetidae* domes are missing. Elevations of these crusts vary from +1.59 m at RHS (overlying a *Strombus* subunit; Fig. 4b: 13) to +2.78 m at RHN (Table 2), where it

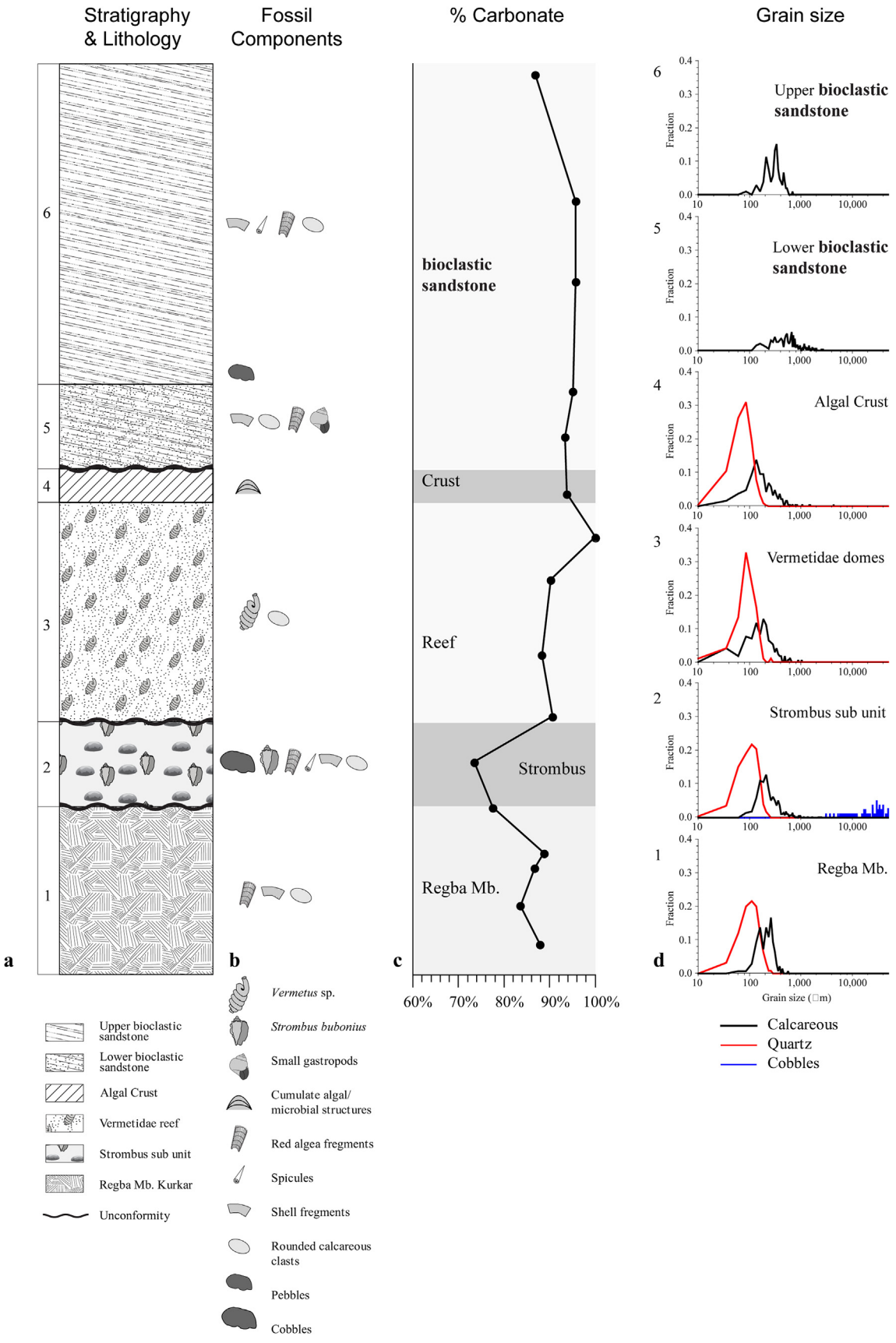

Fig. 5. The generalized type section: a. stratigraphical relations, b. diagnostic fossil assemblages, c. % carbonate; d. the relative percentages of the quartz and the carbonate of the different units and the grain sizes of the two main grain components: the Nile derived quartz and the biogenic carbonates.

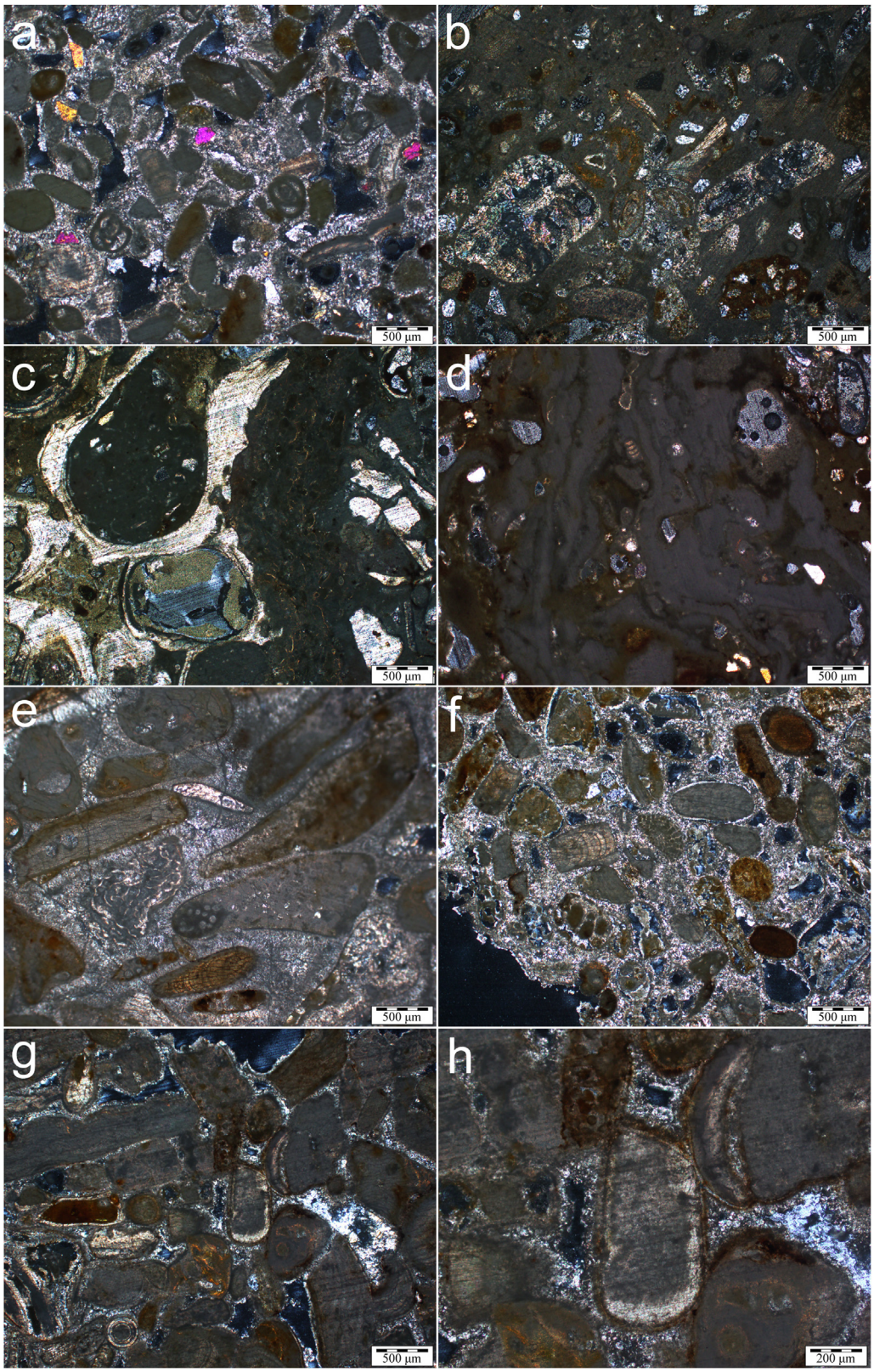

Fig. 6. Photomicrographs showing sedimentological and diagenetic features at the Rosh Hanikra north (RHN) type section: a. Cemented calcarenite of the *Regba* Mb. sandstone, comprised of well sorted fine to medium sand size quartz and calcareous grains, the later include fragments of red algae, varied foraminifera and micritic clasts. Micritic envelopes are present around some of the grains. First generation of isopachous blade cement, followed by a second generation granular cement can be seen. b. Two main size texture categories observed in the subunit: 1) gravel up to boulder size, poorly sorted, poorly rounded varied clasts and large gastropods (*Strombus bubonius*); 2) quartz and well rounded, very poorly sorted calcareous clasts - well sorted, poorly rounded, very fine to fine sand size. Non-selective dissolution features are present and open pores are partially filled with granular cement, possibly drusy and some grains have isopachous blade cement envelopes. c. The *Vermetidae* domes filled with micrite, small gastropods and an assemblage of calcareous clasts and quartz grains. The calcareous clasts are moderately well sorted, well rounded, fine to medium sand size. The quartz grains are well sorted, poorly rounded, very

Table 3
U series ages obtained from the subunits of the study area.

Sample	Sub-sample	Species	Calcite/ Aragonite	232Th pmol g-1	(±) 2σ	230Th pmol g-1	(±) 2σ	238U nmol g-1	(±) 2σ	[230Th/238U] [act.]	(±) 2σ	[234U/238U] [act.]	(±) 2σ	Age Ka	(±) 2σ	$d^{234}U$ Initial	(±) 2σ
Terrace RH South																	
RH-S-1.1	RH-S-1.1 A	Strombus bubonius	C	29.0	0.3	0.080	0.002	6.40	0.02	0.7354	0.021	1.126	0.006	112	6	173	8
	RH-S-1.1B			32.9	0.6	0.079	0.002	6.53	0.01	0.7123	0.020	1.118	0.005	108	5	160	6
	RH-S-1.1 C			30.2	2.7	0.083	0.002	6.84	0.02	0.7123	0.014	1.116	0.006	108	4	157	8
RH-S-1.2	RH-S-1.2 C	Strombus bubonius	C	35.0	1.6	0.065	0.001	5.35	0.01	0.7190	0.015	1.112	0.005	111	4	153	7
	RH-S-1.2 A -II			92.0	0.9	0.059	0.001	4.87	0.02	0.7131	0.011	1.108	0.009	110	3	148	13
	RH-S-1.2 b			59.7	0.6	0.062	0.001	5.31	0.01	0.6910	0.016	1.112	0.007	104	4	150	9
RH-S-1.4	RH-S-1.4-A	Strombus bubonius		105	0.8	0.230	0.002	19.1	0.05	0.7108	0.006	1.117	0.005	108	2	159	7
	RH-S-1.4-B			126	0.9	0.173	0.002	13.9	0.03	0.7333	0.007	1.111	0.004	115	2	154	6
	RH-S-1.4-C			207	1.6	0.157	0.002	12.6	0.03	0.7303	0.008	1.113	0.004	113	2	156	5
RH-S-3.2		hexaplex trunculus	C	28.3	0.6	0.151	0.004	12.4	0.04	0.7161	0.018	1.103	0.005	112	5	141	8
RH-S-3.3	RH-S-3.3	Unidentified vermetid		193	2.4	0.069	0.001	6.53	0.02	0.6214	0.012	1.110	0.008	88	3	141	10
	RH-S-3.3-II	gastropod		179	1.4	0.081	0.002	7.61	0.02	0.6255	0.016	1.104	0.006	90	4	134	8
RH-S-3.4-II		cerithium vulgatum		39.3	0.3	0.117	0.001	10.5	0.02	0.6607	0.004	1.106	0.005	97	1	139	7
RH-S-3.5	RH-S-3.5	cerithium vulgatum		67.0	0.5	0.111	0.001	11.2	0.04	0.5854	0.008	1.101	0.008	82	2	127	10
	RH-S-3.5-II			69.5	0.5	0.124	0.001	10.3	0.03	0.7117	0.008	1.119	0.005	108	2	162	7
Terrace RH North																	
RH-N-2.1		Petaloconchus	Ar = CC	574	3.0	0.086	0.001	6.92	0.02	0.7254	0.010	1.167	0.007	103	3	223	9
RH-N-2.2	RH-N-2.2	Petaloconchus	C = 20	582	4.0	0.143	0.002	10.5	0.03	0.8018	0.012	1.147	0.006	126	4	210	8
	RH-N-2.2-II		−30%	593	2.8	0.065	0.001	4.01	0.01	0.9638	0.009	1.234	0.009	153	4	361	13
RH-N-3.1	RH-N-3.1 A-II	Petaloconchus	C > Ar	352	1.8	0.046	0.000	6.69	0.02	0.3968	0.005	1.153	0.007	46	1	174	8
	RH-N-3.1 A			197	1.2	0.039	0.000	4.96	0.01	0.4580	0.006	1.152	0.004	55	1	178	5
	RH-N-3.1 B			152	0.8	0.035	0.001	8.49	0.02	0.2440	0.005	1.119	0.005	27	1	128	5
	RH-N-3.1 B-II			292	2.0	0.049	0.001	8.36	0.02	0.3409	0.004	1.127	0.006	39	1	142	6
RH-N-3.3		cerithium vulgatum		20.9	0.1	0.095	0.001	19.0	0.07	0.2946	0.003	1.110	0.007	33	1	121	7
RH-N-3.4		cerithium vulgatum		39.2	0.6	0.066	0.001	8.67	0.02	0.4516	0.009	1.125	0.006	55	2	146	7
RH-N-3.5		Boring species		598	8.9	0.035	0.001	5.28	0.01	0.3746	0.015	1.106	0.006	45	2	121	7
RH-N-3.6		Shell		51.8	0.5	0.042	0.001	3.08	0.01	0.7940	0.014	1.098	0.013	136	6	144	19
RH-N-3.7		Shell		63.2	1.1	0.044	0.002	3.51	0.01	0.7410	0.027	1.187	0.007	103	6	251	9

Table 4
Summary of key features in the ice histories used in GIA modelling. The amplitude change of ice volume is expressed in metres equivalent sea level (m.e.s.l.).

Ice history	Ice history based on	Dispersal Pattern (A: ICE-5G (Peltier, 2004), B: 3D ice history (de Boer et al., 2014)	Model interglacial duration (kyr)	Ice volume difference between peak interglacial and present day model ice volume (m.e.s.l.)
1	ICE-5G (Peltier, 2004)	A	4	0
2a	Red Sea RSL (Grant et al., 2014)	A	4	−0.2
2b	Red Sea RSL (Grant et al., 2014)	A	8	−0.2
3a	Red Sea RSL (Grant et al., 2014)	B	4	−0.8
3b	Red Sea RSL (Grant et al., 2014)	B	8	−0.8
4	Algorithmic 3D ice history (de Boer et al., 2014)	B	6	−3.7
5	LR04 (Lisiecki and Raymo, 2005)	A	4	−3.7
6	Global sea level (Waelbroeck et al., 2002)	A	4	−4.5

covers the highest mound-shaped structure.

The bioclastic subunit unconformably overlies the sequence described above. The contact between the bioclastic subunit and the underlying subunits is irregular, wavy, and abrupt. This subunit consists of a set of well-bedded, bioclastic sandstone beds, where the lower is relatively coarse and the upper relatively fine grained and well sorted. The contact between the lower and upper beds is by gradational fining upward. The lower bioclastic sandstone is medium to coarse planar bedded, gently dips seaward, and contains gastropods, vermetids, and bivalves. The upper bioclastic sandstone

fine to fine sand size. d. Undulatory to cumulate algal/microbial structures in the crust engulfing the domes. In between lamina are small gastropods and an assemblage of calcareous clasts and quartz grains. The calcareous clasts include fragmented bivalve and red algae and lithified material. Clasts are elongated, poorly or well-rounded and poorly sorted fine to medium sand size. The quartz grains are well sorted, poorly rounded, very fine to fine sand sized. Granular cement fills mold type pores; non-selective dissolution is also present. e. Fully cemented grainstone in the lower bioclastic sandstone subunit, grains are an assemblage of calcareous clasts and bioclasts, including foraminifera and small gastropods. The calcareous clasts are moderately well sorted, well rounded, medium to coarse sand size fragments of red algae and micritic marital. Several grains exhibit edge dissolution coated by fine micritic envelopes and either fibrous or blade cements; final stage of cementation is granular. f. Partially cemented grainstone in the upper bioclastic sandstone, grains are an assemblage of calcareous clasts and bioclasts, the later include foraminifera and spicules. The calcareous clasts are well sorted, well rounded, fine to medium sand size with fragments of red algae and micritic material, some grains are coated by fine micritic envelopes. Micrite is partially recrystallized, grains are surrounded by partial isopachous cement; non-selective dissolution is also present. g. Poorly cemented grainsstone in the bioclastic sandstone as occurring in the cave: grain size and texture are similar to the lower sandstone sub unit. h. Same sample in higher magnification, edge dissolution and recrystallization can be observed.

is fine to medium planar bedded, and contains gastropods, bivalves, and spicules. The two-bed bioclastic sandstone subunits are exposed from the elevation of the current abrasion platform, where it fills tidal palaeochannels at elevations of +0.9 m at SZ, +1.0 m at HY, and +1.1 m at RHS (Fig. 4a: 2 and Table 2), or as a thick unit overlying the *Regba* Mb. kurkar (Fig. 4b:15 and 4b:16). Maximum elevations of the two bioclastic sandstone beds were measured at +6.45 m in RHS, and +5.7 m in SZ (Fig. 3 and Table 2). In RHN, almost the entire sequence is exposed in man-made excavations (Fig. 4c:17 and 4c:18). The lower bioclastic sandstone bed was also found within the sea-cave in RHN. There, it comprises a 1.1 m thick layer of bioclastic calcarenite with coarse-sand-sized fragments of gastropods and bivalves, cemented by calcite, at elevations varying from +1.5 m at the bottom close to the inlet of the cave, to about +4 m at its uppermost edge within the cave (Fig. 4c 19–21).

3.2. Mineralogy, grain size, micro-analysis

The *Regba* Mb, the *Strombus* subunit, and the *Vermetidae* reef with the algal crust all contain similar grain sizes for the calcareous and for the quartz clasts. The overlaying bioclastic sandstone beds contain only calcareous grains in smaller sizes, and no quartz grains (Fig. 5). Petrographic analysis in thin section reveals that the top of the *Regba* Mb. kurkar is a cemented grainstone (calcarenite) that consists of well-sorted, fine to medium sand size calcareous clasts and quartz grains (Fig. 6a).

The *Strombus* subunit comprises a wide range of clasts in two main size categories in a floatstone texture (*sensu* Embry and Klovan, 1971). The first size category concerns large and poorly sorted, poorly rounded, varied clasts and large gastropods (*Strombus* sp.) suspended in a matrix. The second size category consists of quartz and well-rounded, very poorly sorted calcareous clasts, with very fine to fine sand-sized quartz grains (Fig. 6b).

The *Vermetidae* domes are filled with micrite, small gastropods, and an assemblage of calcareous clasts and quartz grains. Carbonate phase bulk mineralogy consists of 75% calcite and 25% aragonite (Fig. 6c). The crust engulfing the domes is a boundstone that consists of undulatory to cumulate algal/microbial structures. In between laminae are small gastropods and an assemblage of calcareous bioclasts and quartz grains; the bioclasts include remains of foraminifera and small gastropods (Fig. 6d). The foraminiferal assemblage is dominated by *Ammonia* sp.1 (13%), accompanied by *Peneroplis pertusus* (Forskål), *Buccella granulata* (di Napoli Alliata), *Asterigerinata mamilla* (Williamson), *Osangulariella bradyi* (Earland), *Peneroplis planatus* (Fichtel & Moll), *Pseudoschlumbergerina ovata* (Sidebottom), and *Rosalina macropora* (Hofker), each with relative abundances between 5 and 9%. Ostracods are present in low abundances of 6 individuals per gram. Six species were identified, with *Aponesidea reticulata* (Mueller), *Hemicythere arborescens* (Brady), and *Cyprideis torosa* (Jones) accounting for 67% of the ostracod assemblage. All ostracods shells were of reworked adults and disarticulated.

Fully cemented grainstone in the lower bioclastic sandstone subunit becomes partially cemented grainstone in the upper bioclastic sandstone, the later includes also spicules. The carbonate phase bulk mineralogy ranges from 95% calcite (5% aragonite) in the lower bioclastic subunit to 60% calcite (40% aragonite), with fibrous isopachous cement (Figs. 5, 6e and 6f).

3.3. Chronology

The top of the *Regba* sandstone in the study site was OSL dated in one sample at RHN to 215 ± 22ka, which seems to relate it to MIS7. In addition, we have performed U–-Th analyses on several types of fossil samples from the *Strombus* and *Vermetidae* subunits. From RHS, fragments of several *Strombus bubonius* shells were analyzed, while from the northern part mainly *Petaloconchus* samples were analyzed (Table 3). The shells of most of these fossils have been recrystallized from aragonite to calcite, possibly by reaction with fresh water.

We acknowledge that molluscs in general behave as an open system for U-Th dating (e.g. Kaufman et al., 1971) and that the validity of *Strombus bubonius* ages is questioned (Sivan et al., 1999). Moreover, even if the *Strombus* behaved as a closed system while being aragonitic (in the shoreline environment), the recrystallization of the RH *Strombus* from aragonite to calcite may have opened the isotope system. If we assume, however, that the *Strombus* remained a closed U-Th isotope system after recrystallization and removal from the marine environment, then the determined ages might be seen as an approximation of the recrystallization age. To evaluate whether the U-Th data of the (now) calcitic *Strombus* might provide chronological information of some validity, we analyzed several sub-fragments of individual fossils and examined whether these show any systematic variations in the ^{238}U and ^{230}Th concentrations. This approach was recently developed for, and applied to, corals that were recrystallized from aragonite to calcite (Lazar and Stein, 2011; Yehudai et al., Under review). The working hypothesis is that, if several sub-fragments of different *Strombus* specimens collected in different places within the *Strombus* subunit yield similar ages, then this would strongly argue against arbitrary open-system behavior. We then proceed to the next working hypothesis that if U was re-distributed in the skeleton during recrystallization from aragonite to calcite, recrystallization was fast and occurred early in the history of the RH terrace. If this was so, and the samples remained a closed isotope system after recrystallization then we should expect linear scattering in a ^{230}Th versus ^{238}U (activities) variation diagram (Fig. 7a). The slope of that linear trend may then be related to isotope growth since the time of recrystallization (the amount and scattering of ^{230}Th atoms at time of recrystallization should be limited, otherwise no correlation should be expected in Fig. 7a).

Our U and Th isotope data are listed in Table 3. We limit the description and discussion of the data to only the *Strombus bubonius* samples since they appear to yield consistent results, while the other fossils, e.g. the *Vermetidae*, yielded scattered $^{230}Th/^{238}U$ and $^{234}U/^{238}U$ activity ratios that were not suitable for assessment in any systematic manner. U and Th concentrations in the now calcitic *Strombus bubonius* shells are 4.9–19 nmol/g and 29–207 pmol/g, respectively. The *Strombus bubonius* sub-samples of three different fossils collected from different sites in the *Strombus* subunit yielded similar results and plot in a close cluster in the $^{230}Th/^{238}U$-$^{234}U/^{238}U$ evolution diagram (8a and b), almost along an isochron line and close to the seawater evolution line with $^{234}U/^{238}U = 1.15$. Plotting the activity ratios of the samples in the ^{230}Th-^{238}U and ^{234}U-^{238}U plots (Fig. 7a and b respectively) reveals positive correlations that indicate that U was re-distributed in the *Strombus bubonius* samples in some systematic way. We infer that the alteration of the *Strombus bubonius* shells did not significantly shift the $^{234}U/^{238}U$ activity ratios from their original seawater value, and that the isotope system remained closed since the time of recrystallization that caused redistribution of the U in the shell.

Calculating U-Th "single-ages" for the sub-samples (Fig. 8) yielded an average age of 110 ± 8 ka (2σ) and initial $^{234}U/^{238}U$ ratio of 1.157 ± 14, which is around or slightly higher than the open seawater value. The slopes of the sub-samples plotted in the ^{230}Th-^{238}U and ^{234}U-^{238}U diagrams (Fig. 7a and b) are 0.721 and 1.115 respectively, which correspond to a "diagenesis-age" of ~110 ka and initial of ~1.157, similar to the averages of the single calculated ages. Given the manipulations and assumptions involved, we do not use these ages in any other way than to infer a likely MIS5e

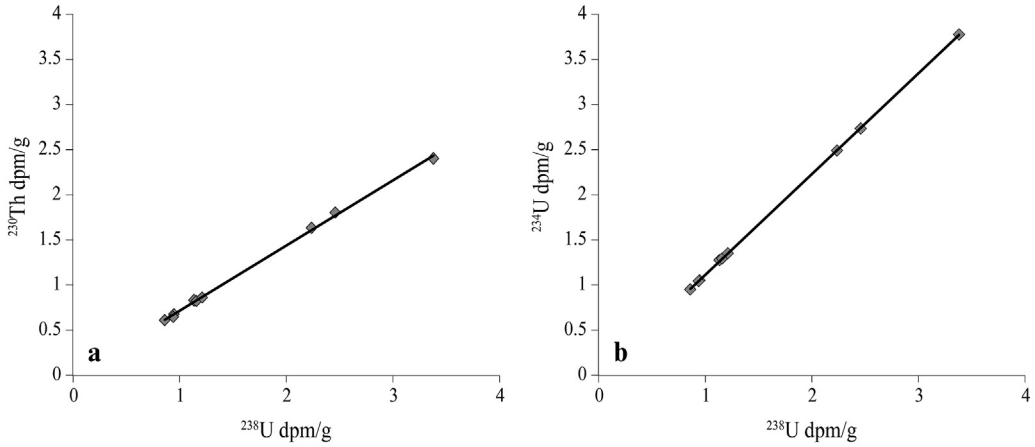

Fig. 7. The sub-samples of the *Strombus bubonius* shells define good linear correlations in the: a. ^{230}Th-^{238}U and b. ^{234}U-^{238}U variation diagrams, where the slopes correspond to ^{230}Th/^{238}U and ^{234}U/^{238}U activities, respectively. Assuming that, during the time of recrystallization from aragonite to calcite, U was redistributed in the recrystallized shell but Th remains intact, the slopes would reflect isotopic ingrowth and can be used to calculate the time of recrystallization. The close to zero intercept in the ^{230}Th-^{238}U diagram may indicate that time of recrystallization is close to the original age of *Strombus bubonius* formation (with aragonite shell).

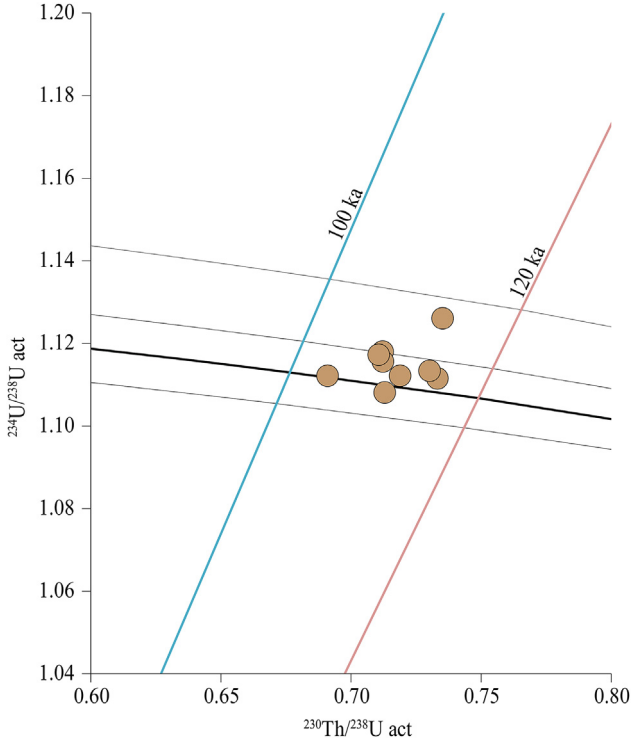

Fig. 8. Distribution of the *Strombus bubonius* shells (sub-fragments) in the ^{230}Th/^{238}U - ^{234}U/^{238}U evolution diagram. Most of the samples scatter along the ~110 ka isochron and close to the seawater evolution line (^{234}U/^{238}U = ~1.15 solid line). This configuration indicates that recrystallization was close to the time of original deposition of the *Strombus bubonius*.

age for the *Strombus* samples, with recrystallization taking place soon after sea-level fell to or below the elevation of the *Strombus* subunit.

3.4. Glacial isostatic correction

As the stratigraphic sequence and available age constraints indicate that the study sequence was deposited during the MIS5e interglacial, we only examine GIA model predictions for times during the interglacial. We define the interglacial on the criterion that ice volume is at, or smaller than, present-day values. This criterion isolates the interglacial period from the prior rapid deglaciation, and from the drop in sea level at the end of the interglacial. It also means that the absolute timing of the interglacial period used by the underlying ice histories is irrelevant; we identify and analyze an interglacial response based solely on ice volume changes in a relative sense.

Our various ice histories (Table 4) allow us to simulate scenarios that include different spatial distributions of ice, different durations of the interglacial, different ice-volume amplitude changes between glaciation and deglaciation, and different ice volumes with respect to present-day across the interglacial. We generate GIA corrections for the beginning of the interglacial period, and for the end of the interglacial period (Table 5). For all ice histories, the GIA correction varies in size across the interglacial with a maximum correction between relative and global mean sea level occurring at the beginning of the interglacial (Figure S3). Given the uncertainty in dating it is difficult to temporally locate the stratigraphic sequence within the interglacial. Hence, our GIA analysis focuses on quantifying the maximum range of GIA corrections possible for RH during MIS5e (range of −1.8 to +5.4). This maximum range is applied to the reconstructed RSL (Table 2) at all time points, although there is an argument for applying the reduced range of GIA corrections generated at the end of an interglacial (Table 5, range of −1.2 to + 2.4) to the youngest RSL indicator.

A sensitivity to ice dispersal pattern and duration of interglacial can be discerned by comparing the results generated by Ice 2a,b with 3a,b. Variations in total global ice volume are held near-constant between the Ice 2 and Ice 3 scenarios, changing only the ice dispersal pattern or duration of interglacial. When we compare Ice 2a with Ice 3a, or Ice 2b with Ice 3b (i.e. varying only the dispersal pattern), the Ice 3 scenarios generate a comparatively larger range of GIA corrections. This is because a larger Eurasian ice sheet, as found in Ice 3, is likely to introduce more intermediate field effects due to GIA.

Despite similarities in dispersal patterns and duration of interglacial, Ice 1, 2a, 5 and 6 generate the full range of potential GIA corrections (which span a range from −1.8 to +5.4 m), indicating that dispersal pattern and interglacial duration are not the only controls on the range of GIA corrections generated. Furthermore, Ice 1, 2a, 2b, 3a and 3b all have near present-day ice volume values through the Last Interglacial, yet generate the full −1.8 to +5.4 range of corrections. This compares with Ice 4, 5 and 6, which have

Table 5
GIA corrections generated by the range of earth models and ice histories used in the GIA modelling.

Ice history	GIA correction at start of interglacial (minimum value and maximum value, given all earth models) (m)	GIA correction at end of interglacial (minimum value and maximum value, given all earth models) (m)
1	0.4: 1.6	−0.1: 0.8
2a	−1.1: 3.1	0.3: 1.6
2b	−1.8: 2.2	0.4: 1.4
3a	1.0: 5.4	1.0: 1.6
3b	−0.1: 5.4	−1.2: 1.4
4	−1.5: 2.0	−0.2: 2.4
5	0.3: 5.4	−1.0: 1.4
6	0.4: 4.9	−0.6: 1.6
Across all	−1.8: 5.4	−1.2: 2.4

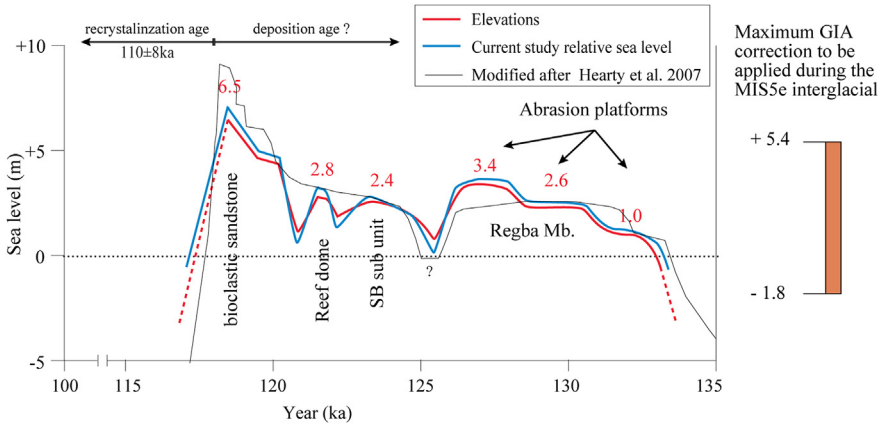

Fig. 9. Pattern of elevations and reconstructed relative sea level during MIS5e from Rosh Hanikra)Galilee coast, Israel). Time axis is tentative since the average age of 110± 8ka is a recrystallization age of the *Strombus bubonius* fossils, probably from the time sea level fall at the end of MIS5e. Reconstructed sea level from this study is compared to the composite curve (grey line) of Hearty et al. (2007) which is based on data from "different sites, regions and ocean basins". The pattern of sea-level change and elevations between the two curves are similar. Although the Rosh Hanikra results lack precise age-control the vertically constrained pattern indicates relative sea level at up to +3.0 m for most of MIS5e interglacial with a peak of about +7 m at the end period. We use GIA modelling to infer global mean sea level from relative sea level during MIS5e. The range of corrections displayed indicates relative sea level at Rosh Hanikra during MIS5e may lie beneath (by up to 5.4 m) or sit above (by up to 1.8 m) global mean sea level. Our modelling indicates that this range of corrections would decrease towards the end of the MIS5e interglacial (and would range between −1.2 m and +2.4 m). However given uncertainty in dating the stratigraphy, we apply the larger range of GIA corrections to this reconstruction.

approximately 4 m less ice through the interglacial than present-day values, and which also generate a −1.8 to +5.4 m range of corrections.

In short, our scenarios may not be comprehensive enough to isolate the factors leading to different GIA predictions in this location, but they generate a range of potential GIA corrections that incorporate uncertainties in choice of Earth model, ice volume, duration of interglacial, and ice dispersal patterns. Ranges of GIA corrections are found for both an early, and a later part of the interglacial. Should more precise dating or further evidence to constrain the duration of the interglacial in this area become available, then the ice history scenarios may be developed further, which would allow discrimination between GIA corrections for the beginning and the end of the interglacial. The results generated here provide first guidance about the likely sensitivities that may be further explored for refining and developing the ice histories.

4. Discussion

The studied sections, and especially the regional type section at Rosh Hanikra (Galilee coast, Israel), provides insight into MIS5e global mean sea level, within a context of regional oceanographic circulation and hydrology of the Mediterranean basin. Today, sea level in the Mediterranean deviates from global sea level due to a variety effects (Pinardi et al., 2014), including: (1) strong net evaporative mass loss that causes a lowering of sea level in the basin relative to the open ocean; (2) mean salinity increase of ~3 psu from west to east related to the net evaporation (e.g., Rohling et al., 2015), which results in saline contraction; (3) mean surface warming of ~3 °C from west to east (e.g., Rohling et al., 2015), which leads to thermal expansion. In addition, sea level is patterned within the basin, with amplitudes in sea level anomalies up to 40 cm (CMEMS, 2011) due to (a) regional gyres and eddies in the sea's circulation that impart dynamic topography, some of it in a more constant form related to long-term stationary gyres and eddies, and some of it transient in relation to moving and/or short-lived eddies; and (b) barometric effects related to atmospheric pressure conditions.

Overall, it appears that persistent atmospheric conditions and circulation changes may cause sea level in the study region to deviate from global sea level by several tens of centimeters. A component of those deviations is short-lived and cancels out when integrated over millennial timescales, but another significant portion is related to long-term persistent conditions that will cause offsets even when integrated over long periods of time. An additional complication during MIS5e arises from the fact that this was a time of exceptionally strong African monsoon intensity, driving large quantities of freshwater influx into the Mediterranean (Rohling et al., 2015 and references therein). This imparts a major departure in the basin's mass balance, salinity, and circulation patterns relative to the present. We therefore recommend considering uncertainties of at least ±1 m to inferences of MIS5e global

sea level from our eastern Mediterranean reconstruction.

In terms of eastern Mediterranean sea-level reconstruction, the sequence for the tectonically stable region of Rosh Hanikra is very promising, given that it comprises a continuous series of sedimentological subunits with clear-cut stratigraphical relationships, and that each subunit indicates sea level with an uncertainty of ≤1 m (Table 2) as summarized by Hearty et al. (2007). The greatest scope for improvement of our reconstruction is in improved age control. Our efforts for the subunits of the ideally situated Rosh Hanikra section were thwarted by almost complete diagenetic alteration of the enclosed fossils. This meant that our age control is limited to identifying that the sequence likely represents MIS5e.

Tectonic stability of the Israeli coast, and notably the Galilee and Carmel sectors where MIS5e units are exposed, has been demonstrated by work in different research disciplines: geology (Sneh, 2000, 2004; Galili et al., 2007), archaeology (Sivan et al., 2001, 2004), and biology (Sivan et al., 2010). We report elevations of MIS5e subunits in that region between +0.8 and + 6.5 m. The implied MIS5e sea level positions of about +1.0 m to about +7 m (Table 2) seem similar to other MIS5e RSL values from stable areas such as the Bahamas, Northeast Yucatan peninsula, Mexico, and Western Australia (Table 1). However, true comparison between different sites would require detailed modelling GIA responses.

The Rosh Hanikra sequence unconformably covers the *Regba* Mb, which has been previously identified as an aeolian deposit that was tentatively ascribed to MIS6 (Sivan et al., 1999). Large-scale cross-bedding within the *Regba* Mb indicates aeolian dunes (Figs. 4a, 3 and 4). However, planar beds at the top of the *Regba* Mb, and their petrographic characteristics, suggest a shallow marine or coastal environment (Table 2). There is a mixture of well-sorted quartz grains and calcareous clasts, which implies winnowing within the depositional environment (Fig. 5c and d). Composition of bioclasts (foraminifera, red algae etc.) suggests reworking of marine carbonates. Micro-sedimentological analyses suggest deposition ranging from shallow subtidal to shore aeolian (Fig. 6a). Therefore, the current study results remain inconclusive in this respect, as they too can reflect both coastal (Pomar, 2001; Vakarelov et al., 2012) and aeolian (Sun et al., 2002) environments. We report a new OSL age of 215 ± 22 ka for the top of the *Regba* Mb, which indicates that its top was deposited in MIS7, rather than MIS6. During MIS6, sea level fell and the area was exposed to terrestrial erosion. The sea-level rise into MIS5e abraded the top of *Regba* Mb. and created three abrasion platforms at elevations of +1.0 m (abraded by the modern MSL), +2.6 m and +3.4 m (Table 2, Figs. 3, 4a: 1 and 2 and 9). These platforms are relatively flat abrasive surfaces, formed in a narrow elevation range closely associated with the level of the sea (Murray-Wallace and Woodroffe, 2014, p.114–115) and cut by tidal channels that suggest relative long sea-level still-stands.

Sea level dropped and rose again, given that the *Strombus* subunit was unconformably deposited over the lowest abrasion platform from ~+0.8 m to a maximum elevation of +2.4 m (Table 2 and Fig. 3) and over Cretaceous chalk at the sea cave. It contains coarse pebbles and abundant remains of fauna, including the characteristic *Strombus bubonius.* The occurrence of *Strombus* fossils up to ~10 cm, along with rhodoliths (coralline algae), and pebbles up to 75 cm, reflects a high wave-energy (probably storm-affected) coastal depositional environment (Bardaji et al., 2009; Dabrio et al., 2011). Multiple cement types, both marine and meteoric, and non-selective dissolution occur through the unit (Fig. 6b), suggesting exposure to meteoric vadose conditions (Ahr, 2008) subsequent to deposition of the sequence (for details see the Fig. 6b caption). These field relationships, combined with sedimentary and micro-analysis data, indicate an early deposition phase in an intertidal environment with enhanced storm activity, with sea levels up to about +2.5 to +3.0 m (Table 2 and Fig. 7), followed by sea-level fall that caused relatively short exposure.

The mound-shaped reef structure (the *Vermetidae* domes) that overlays the *Strombus* subunit mainly contains the reef-building gastropod *Petaloconchus* (Fig. 4b 11 and 12), covered by red coralline algal crusts (rhodolith bioherms) and microbialites. The reef stratum is locally exposed by historical excavations and therefore at present known only from RHN. Vermetid reefs are known from the Middle Miocene to present-day and are used as sea-level indicators. *Petaloconchus* was the major vermetid reef builder in the Mediterranean up to the Holocene when, for unknown reasons, it was almost completely replaced by *Dendropoma* (Vescogni et al., 2008). Since *Petaloconchus* can live up to 30–50 m water depth, it is important to recognize the entire reef assemblage in order to conclude that original water depths were representative of the subtidal to intertidal zone (Vescogni et al., 2008). The mound-shapes (such as those reported here for Rosh Hanikra) have been interpreted as an indication for high-energy shallow-water settings, similar to those of the present-day intertidal *Dendropoma* reefs. The reef unit is fully covered by red coralline algal crusts with a possible microbialite component. In places where the reef is missing, the algal bioherm crust covers the *Strombus* subunit. The depositional conditions for the crust have been interpreted as shallow water (Dabrio et al., 2011). The wave-rippled coarse lamination of the bioherm suggests intertidal deposition, close to mean sea level. The mound-shaped reef and the biogenic crust infer a sea level at about +3 m (Table 2). The benthic foraminiferal species found at RHN inhabit shallow-water, high-energy, quartz-rich, sandy or carbonate-rich, rocky substrates (Lazar, 2007; Hyams-Kaphzan et al., 2008; Avnaim-Katav et al., 2013, 2015). The dominant species *Ammonia* sp., *P. pertusus*, and *B. granulata*, have rather narrow benthic zonation, thriving at water depths between 0 and −6 m (Avnaim-Katav et al., 2013, 2015, 2016). The majority of the foraminiferal assemblage is moderately to poorly preserved and often polished, suggesting wave erosion within a shallow, coastal, high-energy environment, which reduces the inferred water depths to 0–3 m (Avnaim-Katav, 2011; Avnaim-Katav et al., 2013). Low numbers of ostracod species are also characteristic of littoral environments (Maddocks et al., 2004; Avnaim-Katav, 2011). The foraminiferal assemblage from the top mound shape structure, and the poor state of preservation of both the foraminifera and the ostracoda, suggest shallow marine habitats within the subtidal zone. Hence, sea levels for this depositional phase are estimated at +3 m to +4 m (Table 2).

There is an irregular contact between the reef and the overlaying marine calcareous bioclastic sandstone, which formed at elevations between +1.0 m and +6.45 m (Table 2). This suggests that reef formation terminated – likely due to a sea-level fall – and that a subsequent transgression gave rise to deposition of the sandstone sediments. Tidal channels in the lower abrasion platforms are filled with these marine sandstone sediments (Fig. 4a 2). The bedding structure is planar, dipping seaward, and the sediments contain gastropods (including vermetids) and bivalves, implying an intertidal foreshore or intertidal beach-bed environment. A change in sediment source relative to underlying units is most evident by an absence of quartz (Fig. 5 c and d) and a decrease in grain size. Marine conditions are indicated also by the preservation of relatively delicate bioclasts (Ford and Kench, 2012), in particular spicules. The general structure (Fig. 4c 17) and petrographic characteristics (Fig. 6e and f) indicate a change from marine phreatic conditions to a sub-aerial meteoric vadose environment. The upper, finer-grained, marine bioclastic sandstone bed is found up to +6.45 m in RHS, which indicates a short period of relative sea level rise up to +6.5 or +7.0 m (Table 2 and Fig. 9). Following the maximum sea-level rise indicated by the upper marine sandstone

bed, sea level dropped, the coastline retreated offshore, and thereafter only reached the area again in the Late Holocene (Sivan et al., 2001, 2004).

In the Mediterranean, there are no high-resolution fossil coral derived sea-level indicators as the most abundant coral – *Cladocora caespitosa* – occurs at a range of depths down to about 40 m (Kružić and Benković, 2008). The key fossil for MIS5e in the Mediterranean is the gastropod *Strombus bubonius* (*Lentigo latus or Persististrombus latus)*, which is part of the Senegalese fauna. There are indications for earlier terraces bearing *Strombus bubonius* (Zazo et al., 2003) but in the central and eastern Mediterranean they have been found only in the MIS5e (Sivan et al., 1999; Bardaji et al., 2009). Dating methods that have been previously applied to *Cladocora, Strombus*, and other Senegalese species, include U-Th, Amino-Acid Racemisation (AAR), and Optically Stimulated Luminescence (OSL) (Hillaire-Marcel et al., 1996; Hearty et al., 2007; Zazo et al., 2003 and references therein; Bardaji et al., 2009; Mauz et al., 2012).

Sivan et al. (1999) tentatively attributed the *Strombus bubonius*-bearing unit in Israel to MIS5e. An OSL age of 113 ± 5 ka for a sequence along the Carmel coast (Mauz et al., 2012) strengthens the chronostratigraphic attribution to MIS5e. If the suggested average age of 110 ± 8 ka from the present study is accepted as an estimate for the time of recrystallization from aragonite to calcite, then this again supports the MIS5e interpretation.

The MIS5e elevations between about 0 and + 7 m found here are similar to those in other RSL reconstructions (Table 1 and Long et al., 2015 and references therein), and in particular to those based on coastal structures (Hearty et al., 2007 and references therein; Murray-Wallace and Woodroffe, 2014, p. 286). For better comparison, we performed an initial evaluation of glacial isostatic adjustment responses in the research area during the MIS5e. Results indicate that the magnitude of the GIA correction during MIS5e likely ranges between −1.8 m and +5.4 m, given a range of possible variations in Earth and ice-history parameters. The magnitude of the GIA correction changes at each time point through the interglacial, and these "maximum correction" values do not reflect variations in global ice volume within the MIS5e time window.

Our method of combining results generated by multiple ice histories allows us to explore a range of potential GIA corrections without having precisely dated sea level indicators. The magnitude of the required GIA correction reduces across the interglacial with the GIA correction at the end of the interglacial ranging between −1.2 and +2.4 m. It is possible that this is the more appropriate GIA correction to apply to the youngest reconstructed RSL indicator, and this would constrain global mean sea level during the sea level jump at the end of the interglacial to being within 5.8 m and 9.4 m. All ice histories used in this analysis gain or lose ice-volume concurrently between the two hemispheres. Given the level of complexity evidenced in the stratigraphic record for Rosh Hanikra, this analysis may be further developed by offsetting the phasing of melt from Laurentia, Greenland, and the Antarctic ice sheets, and by incorporating a more variable Eurasian ice sheet.

The study region's continuous MIS5e sequence and tectonic stability make it ideal for extracting reliable relative sea level (RSL) information. The sequence overlies three abrasion platforms indicating that the first MIS5e phase was erosive. From this we infer a relatively extended period of time in which sea levels were up to about +3.5 m. Later in the MIS5e period, the sedimentological and palaeontological data indicate reliable sea level rises and falls with a final jump in RSL of up to +7 m. The current study presents a pattern of fluctuating sea level as found in both intermediate and far-field sites (as presented by Hearty et al., 2007) and provides constraints on the elevations of sea-level change vital for reconstructions of past ice sheet instability.

5. Conclusions

1. A micro-tidal regime and tectonic stability make the study area a good target for high-resolution reconstruction of relative sea-level changes (RSL).
2. The local stratigraphy combined with previously published ages and proposed recrystallization ages of *Strombus* fossils attribute the exposed sequence of the Galilee coast to the Last Interglacial, MIS5e.
3. A sequence of three subunits is identified: (a) a basal subunit of gravels that contain *Strombus bubonius*, indicative of a stormy intertidal to super-tidal regime; (b) a middle subunit of *Vermetidae* reefs that represent a shallow, sub-tidal to intertidal environment, covered by algal crust; and (c) an upper subunit that consists of two beds of coarse to medium, and fine-grained bioclastic sandstones, respectively, which probably were deposited in a shallow sub-tidal environment. The sequence covers three abrasion platforms cut by tidal channels filled with MIS5e sediments at elevations of +0.8, +2.6, and +3.4 m.
4. The coastal structures in Rosh Hanikra support a reliable RSL reconstruction, with a stratigraphic uncertainty of ≤ 1 m, ranging between +1.0 m and +7 m. For most of the MIS5e period, we find that RSL stood between +1.0 m and +3.5 m, with several sea-level regressions to < +1 m. During the final episode of deposition, likely toward the end of MIS5e, RSL reached +7 m or higher.
5. We use GIA modelling to infer that GMSL was between −0.8 m and +8.7 m for most of the MIS5e period. For the reconstructed jump in sea level thought to have occurred at the end of MIS5e we infer GMSL between 5.8 m and 9.4 m. We suggest an additional ±1 m uncertainty on those values to account for deviations between Mediterranean mean sea level and global mean sea level due to local Mediterranean processes.

Acknowledgments

The authors would like to thank H. K. Mienis of the Mollusc Collection, Zoological Museum, Tel Aviv University, and the Mollusc Collection, Hebrew University of Jerusalem, for his significant contribution in identifying the species, and Dr. N. Porat, from the Israeli Geological Survey (IGS) for the OSL dating of the Regba Mb. Thanks to Neta Bar for the U-Th isotopes analysis. Thanks are also due to Noga Yoselevich of the Cartography Laboratory of the Department of Geography and Environmental Studies, University of Haifa, for the graphics. Dr. Sisma-Ventura acknowledges post-doctoral funding by the Israel Science Foundation (ISF) and the University of Haifa. E.J.R, F.H.W, and M.E.T acknowledge support from the UK Natural Environment Research Council (NERC) consortium project iGlass (NE/1009906/1 and NE/1008365/1), and E.J.R. acknowledges support by Australian Laureate Fellowship FL120100050.

Appendix A. Supplementary data

Supplementary data related to this article can be found at http://dx.doi.org/10.1016/j.quascirev.2016.06.001.

References

Ahr, W., 2008. Geology of Carbonate Reservoirs. John Wiley & Sons, Hoboken.
Andrews, J.E., Porbnan, C., Rcme, P.J., Leeder, M.R., Kramers, j.D., 2007. Sub-orbital sea-level change in early MIS 5e: new evidence from the Gulf of Corinth Greece. Earth Planet. Sci. Lett. 259, 457–468.
Athersuch, J., Horne, D.J., Whittaker, J.E., 1989. Marine and brackish water Ostracods (Superfamilies Cypridacea and Cytheracea). In: Kermack, D.M., Barnes, R.S.K. (Eds.), Synopses of the British Fauna. E. J. Brill, Leiden, p. 343.

Avnaim-Katav, S., 2011. Chronostratigraphy and Paleo-environments: Reconstruction of Quaternary Subsurface Successions, Southern Haifa Bay. PhD thesis. University of Haifa (in Hebrew, English abstract, 242 pp.).
Avnaim-Katav, S., Almogi-Labin, A., Sandler, A., Sivan, D., 2013. Benthic foraminifera as paleoenvironmental indicators during the last million years in the eastern Mediterranean inner shelf. Palaeogeogr. Palaeoclimatol. Palaeoecol. 386, 512–530.
Avnaim-Katav, S., Hyams-Kaphzan, O., Milker, Y., Almogi-Labin, A., 2015. Bathymetric zonation of modern shelf benthic foraminifera in the Levantine Basin, eastern Mediterranean Sea. J. Sea Res. 99, 97–106.
Avnaim-Katav, S., Milker, Y., Schmiedl, G., Sivan, D., Hyams-Kaphzan, O., Sandler, A., Almogi-Labin, A., 2016. Impact of eustatic and tectonic processes on the southeastern Mediterranean shelf: Quantitative reconstructions using a foraminiferal transfer function. Mar. Geol. 376, 26–38.
Bar-Yosef, O., 1998. The chronology of the middle paleolithic of the levant. In: Akazawa, T., Aoki, K., Bar-Yosef, O. (Eds.), Neandertals and Modern Humans in Western Asia. Plenum press, new York, pp. 39–56.
Bar-Yosef, O., 2007. The Game of Dates: Another Look at the Levantine Middle Paleolithic chronology.the IV Congress on Archaeology, Faro. University of Algarve, Portugal (From the Mediterranean basin to the Portuguese Atlantic shores. Papers to honor Anthony Marks).
Bardají, T., Goy, J.L., Zazo, C., Hillaire-Marcel, C., Dabrio, C.J., Cabero, A., Ghaleb, B., Silva, P.G., Lario, J., 2009. Sea level and climate changes during OIS 5e in the Western Mediterranean. Geomorphology 104, 22–37.
Blanchon, P., Eisenhauer, A., Fietzke, J., Liebetrau, V., 2009. Rapid sea-level rise and reef back-stepping at the close of the Last Interglacial highstand. Nature 458, 881–884.
Chen, J.H., Curran, H.A., White, B., Wasseburg, G.J., 1991. Precise chronology of the Last Interglacial period: 234-230U–Th data from fossil coral reefs in the Bahamas. Geol. Soc. Am. Bull. 103, 82–97.
Cimerman, F., Langer, M.R., 1991. Mediterranean Foraminifera. Academia Scientarium et Aritium Slovenica, Dela, Opera 30, Classis IV: Historia Naturalis (118 pp., 93 pl.).
CMEMS, 2011. The Ssalto/Duacs Altimeter Products Were Produced and Distributed by the Copernicus Marine and Environment Monitoring Service (CMEMS). Data accessed:http://www.aviso.altimetry.fr/en/data/data-access/las-live-access-server/lively-data/2011/feb-10-2011-high-mediterranean-sla.html. http://www.marine.copernicus.eu (accessed DATE).
Colleoni, F., Wekerle, C., Näslund, J.-O., Brandefelt, J., Masina, S., 2016. Constraint on the penultimate glacial maximum Northern Hemisphere ice topography (≈140 kyrs BP). Quat. Sci. Rev. 137, 97–112.
Dabrio, C.J., Zazo, C., Cabero, A., Goy, J.L., Bardají, T., Hillaire-Marcel, C., González-Delgado, J.A., Lario, J., Silva, P.G., Borja, F., García-Blázquez, A.M., 2011. Millennial/submillennial scale sea-level fiuctuations in western Mediterranean during the second highstand of MIS 5e. Quat. Sci. Rev. 30, 335–346.
de Boer, B., Stocchi, P., van de Wal, R.S.W., 2014. A fully coupled 3-D ice-sheet sea-level model: algorithm and applications: Geosci. Model. Dev. 7, 2141–2156.
Dorale, J.A., Onac, B.P., Fornos, J.J., Gines, J., Gines, A., Tuccimei, P., Peate, D.W., 2010. Sea-level highstand 81,000 years ago in Mallorca. Science 327, 860–863.
Dumas, B., Guérèmy, P., Raffy, J., 2005. Evidence for sea-level oscillations by the «characteristic thickness» of marine deposits from raised terraces of Southern Calabria (Italy). Quat. Sci. Rev. 24, 2120–2136.
Dumas, B., Hoang, C.T., Raffy, J., 2006. Record of MIS 5 sea-level highstands based on U/The dated coral terraces of Haiti. Quat. Int. 145–146, 106–118.
Dutton, A., Lambeck, K., 2012. Ice volume and Sea level during the last interglacial. Science 337, 216–219. http://dx.doi.org/10.1126/science.1205749.
Dutton, A., Carlson, A.E., Long, A.J., Milne, G.A., Clark, P.U., DeConto, R., Horton, B.P., Rahmstorf, S., Raymo, M.E., 2015. Sea-level rise due to polar ice-sheet mass loss during past warm periods. Science 349, 6244. http://dx.doi.org/10.1126/science.aaa4019.
Emiliani, C., 1955. Pleistocene temperatures. J. Geol. 63, 538–578.
Embry, A.F., Klovan, J.E., 1971. A Late Devonian reef tract on northeastern Banks Island, NWT. Bull. Can. Petroleum Geol. 19, 730–781.
Fairbanks, R.G., 1989. A 17,000-year glacio-eustatic sea level record: influence of glacial melting rates on the Younger Dryas event and deep-ocean circulation. Nature 342 (6250), 637–642.
Farrell, W.E., Clark, J.A., 1976. On Postglacial Sea level. Geophys. J. R. Astron. Soc. 46 (3), 647–667.
Flügel, E., 2010. Microfacies of Carbonate Rocks. Springer, Berlin, Heidelberg.
Ford, M.R., Kench, P.S., 2012. The durability of bioclastic sediments and implications for coral reef deposit formation. Sedimentology 59, 830–842.
Frenzel, P., Boomer, I., 2005. The use of ostracods from marginal marine, brackish waters as bioindicators of modern and Quaternary environmental change. Palaeogeogr. Palaeoclimatol. Palaeoecol. 225, 68–92.
Galili, E., Zviely, D., Ronen, A., Mienis, H.K., 2007. Beach deposits of MIS 5e high sea stand as indicators for tectonic stability of the Carmel coastal plain. Isr. Quat. Sci. Rev. 26, 2544–2557.
Grant, K.M., Rohling, E.J., Bar-Matthews, M., Ayalon, A., Medina-Elizalde, M., Bronk Ramsey, C., Satow, C., Roberts, A.P., 2012. Rapid coupling between ice volume and polar temperature over the past 150 kyr. Nature 491, 744–747.
Grant, K.M., Rohling, E.J., Ramsey, C.B., Cheng, H., Edwards, R.L., Florindo, F., Heslop, D., Marra, F., Roberts, A.P., Tamisiea, M.E., Williams, F., 2014. Sea-level variability over five glacial cycles. Nat. Commun. 5, 744–747.
Hearty, P.J., Miller, G.H., Stearns, C.E., Szabo, B.J., 1986a. Aminostratigraphy of Quaternary shorelines in the Mediterranean basin. Geol. Soc. Am. Bull. 97, 850–858.
Hearty, P.J., Bonfigio, L., Violanti, D., Szabo, B.J., 1986b. Age of late Quaternary marine deposits of southern Italy determined by aminostratigraphy, faunal correlation and uranium-series dating. Rev. Ital. Paleontol. Stratigr. 92 (1), 149–164.
Hearty, P.J., 1987. New data on the Pleistocene of Mallorca. Quat. Sci. Rev. 6, 254–257.
Hearty, P.J., Neumann, A.C., 2001. Rapid sea level and climate change at the close of the Last Interglaciation (MIS 5e): evidence from the Bahama Islands. Quat. Sci. Rev. 20, 1881–1895.
Hearty, P.J., Hollin, J.T., Neumann, A.C., O'Leary, M.J., McCulloch, M., 2007. Global sea-level fluctuations during the Last Interglaciation (MIS 5e). Quat. Sci. Rev. 26, 2090–2112.
Hibbert, F.D., Rohling, E.J., Dutton, A., Williams, F.H., Chutcharavan, P.M., Zhao, C., Tamisiea, M.E., 2016. Coral indicators of past sea-level change: a global repository of U-series dates benchmarks. Quat. Sci. Rev. 145, 1–56.
Hillaire-Marcel, C., Carro, O., Causse, C., Goy, J.-L., Zazo, C., 1986. The U dating of Stroinbus bubonius-bearing marine terraces in southeastern Spain. Geology 14, 613–616.
Hillaire-Marcel, C., Gariépy, C., Ghaleb, B., Goy, J.L., Zazo, C., Cuerda, J., 1996. U-series measurements in Tyrrhenian deposits from Mallorca: further evidence for two last-interglacial high sea-levels in the Balearic Islands. Quat. Sci. Rev. 15, 53–62.
Hoang, C.-T., Hearty, P.J., 1989. A comparison of geochronological methods from the "Il Fronte Formation", Puglia, Italy and Son Grauet, Mallorca, Spain. Isot. Geosci. 79 (4), 317–323.
Hottinger, L., Halicz, E., Reiss, Z., 1993. Recent Foraminiferida from the Gulf of Aqaba, Red Sea, 33. Opera Sazu, Ljubljana (179 pp., 230 pls.).
Hyams-Kaphzan, O., Almogi-Labin, A., Sivan, D., Benjamini, C., 2008. Benthic foraminifera assemblage change along the southeastern Mediterranean inner shelf due to fall-off of Nile-derived siliciclastics. Neues Jahrb. Geol. Paläontologie-bhandlungen 248, 315–344.
Israelson, C., Wohlfarth, B., 1999. Timing of the last-interglacial high sea level on the Seychelles Islands, Indian Ocean. Quat. Res. 51, 306–316.
Jones, R.W., 1994. The Challenger Foraminifera. Oxford University Press. Natural History Museum Pub., London (149 pp., 115 pls.).
Kaufman, A., Broecker, W.S., Ku, T.-L., Thurber, D.L., 1971. The status of U-series methods of dating molluscs. Geochim. Cosmochim. Acta 35, 1155–1183.
Kopp, R.E., Simons, F.J., Mitrovica, J.X., Adam, C., Maloof, A.D., Oppenheimer, M., 2009. Probabilistic assessment of sea level during the last interglacial stage. Nature 462, 863–867.
Kružić, P., Benković, L., 2008. Bioconstructional features of the coral Cladocora caespitosa (Anthozoa, Scleractinia) in the Adriatic Sea (Croatia). Mar. Ecol. 125–139.
Lambeck, K., Purcell, A., Funder, S., Kjær, K., Larsen, E., Möller, P., 2006. Constraints on the Late Saalian to early Middle Weichselian ice sheet of Eurasia from field data and rebound modelling. Boreas 35 (3), 539–575.
Lazar, S., 2007. Recent and Late Pleistocene Carbonate-rich Sediments in the Mediterranean Shelf of Israel: Sedimentary, Biogenic and Genetic Analysis. Geological Survey Report GSI/08/2007. (In Hebrew, English abstract).
Lazar, B., Stein, M., 2011. Freshwater on the route of hominids out of Africa revealed by U-Th in Red Sea Corals. Geology 39, 1067–1070.
Lisiecki, E.L., Raymo, E.M., 2005. A Pliocene-Pleistocene stack of 57 globally distributed benthic δ18O records. Paleoceanography 20 (1). http://dx.doi.org/10.1029/2004PA001071.
Long, A.J., Barlow, N.L.M., Busschers, F.S., Cohen, K.M., Gehrels, W.R., Wake, L.M., 2015. Near-field sea-level variability in northwest Europe and ice sheet stability during the Last Interglacial. Quat. Sci. Rev. 126, 26–40.
Marino, G., Rohling, E.J., Rodríguez-Sanz, L., Grant, K.M., Heslop, D., Roberts, A.P., Stanford, J.D., Yu, J., 2015. Bipolar seesaw control on Last Interglacial sea level. Nature 522, 197–201. http://dx.doi.org/10.1038/nature14499.
Maddocks, R., Rosenfeld, A., Honigstein, A., 2004. Holocene Ostracods from the Continental Shelf and Slope of Northern Israel. A Preliminary Report on the Ostracods Assemblages. Report GSI/10/2004. Geological Survey of Israel, Jerusalem.
Mauz, B., Fanelli, F., Elmejdoub, N., Barbieri, R., 2012. Coastal response to climate change: Mediterranean shorelines during the Last Interglacial (MIS 5). Quat. Sci. Rev. 54, 89–98. http://dx.doi.org/10.1016/j.quascirev.2012.02.021.
Medina-Elizalde, M., 2013. A global compilation of coral sea-level benchmarks: implications and new challenges. Earth Planet. Sci. Lett. 362 (0), 310–318.
Milne, G.A., Mitrovica, J.X., 2008. Searching for eustasy in deglacial sea-level histories. Quat. Sci. Rev. 27 (25–26), 2292–2302.
Mischke, M., Almogi-Labin, A., Al-Saqarat, B., Rosenfeld, A., Elyashiv, H., Boomer, I., Stein, M., Lev, L., Ito, E., 2014. An expanded ostracod-based conductivity transfer function for climate reconstruction in the Levant. Quat. Sci. Rev. 93, 91–105.
Moore, C.H., 1989. Carbonate Diagenesis and Porosity, Developments in Sedimentology. Elsevier, Amsterdam.
Muhs, D.R., Kennedy, G.L., Rockwell, T.K., 1994. Uranium-series ages of marine terrace corals from the Pacific coast of North America and implications for last-interglacial sea level history. Quat. Res. 42, 72–87.
Muhs, D.R., Simmons, K.R., Steinke, B., 2002. Timing and warmth of the Last Interglacial period: new U-series evidence for Hawaï and Bermuda and a new fossil compilation for North America. Quat. Sci. Rev. 21, 1355–1383.
Murray-Wallace, C.V., Woodroffe, C.D., 2014. Quaternary Sea-level Changes: a Global Perspective. Cambridge University Press, Cambridge, p. 484.
Neumann, A.C., Hearty, P.J., 1996. Rapid sea-level changes at the close of the Last Interglacial (substage 5e) recorded in the Bahamian island geology. Geology 24 (9), 775–778.

O'Leary, M.J., Hearty, P.J., Thompson, W.G., Raymo, M.E., Mitrovica, J.X., Webster, J.M., 2013. Ice sheet collapse following a prolonged period of stable sea level during the Last Interglacial. Nat. Geosci. 6 (9), 796–800. DOI: org/10.1038/ngeo1890L3.
Peltier, W.R., 2004. Global glacial isostasy and the surface of the ice-age Earth: the ICE-5G (VM2) model and GRACE. Annu. Rev. Earth Planet. Sci. 32, 111–149.
Pomar, L., 2001. Types of carbonate platforms : a genetic approach. Basin Res. 13 (3), 313–334.
Pavlopoulos, K., Kapsimalis, V., Theodorakopoulou, K., Panagiotopoulos, I.P., 2012. Vertical displacement trends in the Aegean coastal zone (NE Mediterranean) during the Holocene assessed by geo-archaeological data. Holocene 22 (6), 717–728.
Pinardi, N., Bonaduce, A., Navarra, A., Dobricic, S., Oddo, P., 2014. The mean sea level equation and its application to the Mediterranean Sea. J. Clim. 27, 442–447.
Pool, A.J., Shimmield, G.B., Robertson, A.H.F., 1990. Late Quaternary uplift of the Troodos ophiolite, Cyprus: uranium series dating of Pleistocene coral. Geology 18, 894–897.
Reiss, Z., Halicz, E., Luz, B., 1999. Late-Holocene foraminifera from the SE Levantine Basin. Isr. J. Earth Sci. 48, 1–27.
Rodríguez-Vidal, J., Cáceres, L.M., Abad, M., Ruíz, F., Martínez-Aguirre, A., 2007. Morphosedimentary evidence of the Last Interglacial Maximum on the coast of Governor's Beach, Gibraltar. Geogaceta 42, 107–110.
Rohling, E.J., Grant, K., Hemleben, C.H., Siddall, M., Hoogakker, B.A.A., Bolshaw, M., Kucera, M., 2008. High rates of sea-level rise during the Last Interglacial period. Nat. Geosci. 1, 38–42.
Rohling, E.J., Grant, K., Bolshaw, M., Roberts, A.P., Siddall, M., Hemleben, Ch, Kucera, M., 2009. Antarctic temperature and global sea level closely coupled over the past five glacial cycles. Nat. Geosci. 2, 500–504.
Rohling, E.J., Foster, G.L., Grant, K.M., Marino, G., Roberts, A.P., Tamisiea, M.E., Williams, F., 2014. Sea-level and deep-sea-temperature variability over the past 5.3 million years. Nature 508, 477–482.
Rohling, E.J., Marino, G., Grant, K.M., 2015. Mediterranean climate and oceanography, and the periodic development of anoxic events (sapropels). Earth Sci. Rev. 143, 62–97.
Sanlaville, P., 1971. Sur le tyrrhènien Libanais. Quaternaria XV, 239–248.
Schellmann, G., Radtke, A., 2004. A revised morpho-and chronostratigraphy of the Late and Middle Pleistocene coral reef terraces on Southern Barbados (West Indies). Earth Sci. Rev. 64, 157–187.
Sgarrella, F., Moncharmont-Zei, M., 1993. Benthic foraminifera of the Gulf of Naples (Italy): systematics and autoecology. Boll. della Soc. Paleontol. Ital. 32, 145–264.
Siddall, M., Rohling, E.J., Almogi-Labin, A., Hemleben, C.H., Meischner, D., Schmelzer, I., Smeed, D.A., 2003. Sea-level fluctuations during the last glacial cycle. Nature 423, 853–858.
Sivan, D., 1996. Paleogeography of the Galilee Coastal Plain during the Quaternary. Geological Survey of Israel Report 18/96. [In Hebrew, English summary].
Sivan, D., Gvirtzman, G., Sass, E., 1999. Quaternary stratigraphy and paleogeography of the Galilee coastal plain, Israel. Quat. Res. 51, 280–294.
Sivan, D., Wdowinski, S., Lamback, K., Galili, E., Raban, A., 2001. Holocene sea-level changes along the Mediterranean coast of Israel, based on archaeological observations and numerical model. Palaeogeogr. Palaeoclimatol. Palaeoecol. 167, 101–117.
Sivan, D., Lambeck, K., Toueg, R., Raban, A., Porat, Y., Shirman, B., 2004. Ancient coastal wells of Caesarea Maritima, Israel, an indicator for sea level changes during the last 2000 years. Earth Planet. Sci. Lett. 222, 315–330.
Sivan, D., Schattner, U., Morhange, C., Boaretto, E., 2010. What can a sessile mollusk tell about the Neotectonics of Eastern Mediterranean? Earth Planet. Sci. Lett. 296 (3–4), 451–458.
Sneh, A., 2000. Faulting in the coastal plain of Israel during the Late Quaternary, re-examined. Isr. J. Earth Sci. 49, 21–29.
Sneh, A., 2004. Geological Map of Israel, Sheet 1-IV, Naharia. Scale 1:50,000 Geological Survey of Israel, Jerusalem.
Stein, M., Wassrburg, G.J., Chen, J.H., Zhu, Z.R., Bloom, A., Chappell, J., 1993. TIMS U-series dating and stable isotopes of the Last Interglacial event in Papua New Guinea. Geochim. Cosmochim. Acta 57, 2541–2554.
Stirling, C.H., Esat, T.M., Lambeck, K., McCulloch, M.T., 1998. Timing and duration of the Last Interglacial: evidence for a restricted interval of widespread coral reef growth. Earth Planet. Sci. Lett. 160, 745–762.
Sun, D., Bloemendal, J., Rea, D.K., Vandenberghe, J., Jiang, F., 2002. Grain-size distribution function of polymodal sediments in hydraulic and aeolian environments, and numerical partitioning of the sedimentary components. Sediment. Geol. 152, 263–277.
Svendsen, J., Alexanderson, H., Astakhov, V.I., Demidov, I., Dowdeswell, J.A., Funder, S., Gataullin, V., Henriksena, M., Hjort, C., Houmark-Nielsen, M.,W., Hubberten, H., Ingóllfsson, Ó. l., Jakobsson, M., Kjæri, K.H., Larsen, E., Lokrantz, H., Lunkka, J.P., Lysa, A., Mangeruda, J., Matiouchkov, A., Murray, A., Möller, P., Niessen, F., Nikolskaya, O., Polyak, L., Saarnisto, M., Siegert, C., Siegert, M.J., Spielhagen, R.F., Steins, R., 2004. Late Quaternary ice sheet history of northern Eurasia. Quat. Sci. Rev. 23 (11–13), 1229–1271.
Taviani, M., 2014. Unpersisting Persististrombus: a Mediterranean story. Vieraea 42, 9–18.
Torfstein, A., Haase-Schramm, A., Waldmann, N., Kolodny, Y., Stein, M., 2009. U-series and oxygen isotope chronology of Lake Amora, Dead Sea basin. Geochom. Cosmochim. Acta 73, 2603–2630.
Tucker, M.E., Wright, V.P., 1990. Carbonate Sedimentology. Blackwell Sci., Oxford, p. 482.
Tuccimei, P., Ginés, J., Delitala, M.C., Ginés, A., Gràcia, F., Fornós, J.J., Taddeucci, A., 2006. High precision U-series data from phreatic overgrowths on speleothems. Z. Geomorphol. 50 (1), 1–21.
Vakarelov, B.K., Ainsworth, R.B., MacEachern, J.A., 2012. Recognition of wave-dominated, tide-influenced shoreline systems in the rock record: variations from a microtidal shoreline model. Sediment. Geol. 279, 23–41.
Vaks, A., Bar-Matthews, M., Ayalon, A., Matthews, A., Halicz, L., Frumkin, A., 2007. Desert speleothems reveal climatic window for African exodus of early modern humans. Geology 35, 831–834.
Vescogni, A., Bosellini, R.F., Reuter, M., Brachert, C.T., 2008. Vermetid reefs and their use as palaeo bathymetric markers: new insights from the Late Miocene of the Mediterranean (Southern Italy, Crete). Palaeogeogr. Palaeoclimatol. Palaeoecol. 267, 89–101.
Waelbroeck, C., Labeyrie, L., Michel, E., Duplessy, J.C., McManus, J.F., Lambeck, K., Balbon, E., Labracherie, M., 2002. Sea-level and deep water temperature changes derived from benthonic foraminifera isotopic records. Quat. Sci. Rev. 21, 295–305.
Wright, V.P., 1992. A revised classification of limestones. Sediment. Geol. 76, 177–185. http://dx.doi.org/10.1016/0037-0738(93)90059-E.
Yehudai, M., Lazar, B., Bar, N., Agnon, A., Shaked, Y., Stein, M., 2016. U-Th Dating of Calcitic Corals from the Gulf of Aqaba (Under review).
Zazo, C., Goy, J.L., Hillaire-Marcel, C., Gillot, P.Y., Soler, V., González-Delgado, J.A., Dabrio, C.J., Ghaleb, B., 2002. Raised marine sequences of Lanzarote and Fuerteventura revisitedda reappraisal of relative sea-level changes and vertical movements in the eastern Canary Islands during the Quaternary. Quat. Sci. Rev. 21, 2019–2046.
Zazo, C., Goy, J.L., Dabrio, C.J., Bardají, T., Hillaire-Marcel, C., Ghaleb, B., González-Delgado, J.A., Soler, V., 2003. Pleistocene raised marine terraces of the Spanish Mediterranean and Atlantic coasts: records of coastal uplift, sea-level highstands and climate changes. Mar. Geol. 194, 103–133.
Zazo, C., Goy, J.L., Dabrio, C.J., Lario, J., González-Delgado, J.A., Bardají, T., Hillaire-Marcel, C., Cabero, A., Ghaleb, B., Borja, F., Silva, P.G., Roquero, E., Soler, V., 2013. Retracing the Quaternary history of sea-level changes in the Spanish Mediterranean–Atlantic coasts: geomorphological and sedimentological approach. Geomorphology 196, 36–49.